Theoretical analysis of orbital and correlation effects on the electronic absorption spectrum of the MnS_4 center in zinc-blende crystals

J. W. Richardson
Department of Chemistry, Purdue University, West Lafayette, Indiana 47907
and Laboratory of Chemical Physics, University of Groningen, Nijenborgh 16, NL 9747 AG Groningen, The Netherlands

G. J. M. Janssen*
Laboratory of Chemical Physics and Materials Science Center, University of Groningen, Nijenborgh 16, NL 9747 AG Groningen, The Netherlands
(Received 6 June 1988)

Optical excitation energies ascribed to the Mn^{2+} center in ZnS:Mn are calculated from Gaussian-based self-consistent-field (SCF) molecular orbitals (MO's) obtained for the tetrahedral MnS_4^{6-} cluster at three Mn-S distances in a static external potential, followed by a detailed investigation of two levels of electron correlation effects. The first level includes only configuration interaction (CI) among the ligand field (LF) d^5 states plus other intra-d-shell contributions by the empirical correlation-energy-correction method (CEC), which is formally equivalent to the intermediate-crystal-field (CF) model. The second level extends the CI to include a large manifold of cluster S→Mn relaxed charge-transfer (RCT) states. At the LF-CI+CEC level, the relative separations among, and the overall width of, the six lowest quartets agree closely with the four bands observed in the spectrum. However, contrary to usual assignments, $b\,^4T_1(^4P)$ is found below $b\,^4T_2(^4D)$, and all quartets are obtained about 0.5 eV too high relative to $^6A_1$. The delocalization effects in the MO's are noticeably smaller than obtained from empirical CF fits to the spectrum. At the second level, CI mixing with the RCT states introduces important changes and interactions not properly encompassed by the orbital-based LF parametrization schemes. This CI depresses the quartet levels almost uniformly down by 0.2 eV relative to $^6A_1$. The order of $b\,^4T_2$ and $b\,^4T_2$ and $b\,^4T_1$ is reversed and now agrees with the usual assignments. Finally these various results are discussed in comparison to less quantitative models in which extended interactions with the host are considered. A degree of similarity between the two formulations is established which gives further justification to the model as used herein.

I. INTRODUCTION

Interest in electronic characteristics of the Mn^{2+} ion situated at tetrahedral sites in chalcogenide structures has been renewed recently in connection with studies of optical and magnetic properties of Mn-doped II-VI compound semimagnetic (or "diluted magnetic") semiconductors.[1] Although many features of the absorption spectra observed have been semiquantitatively discussed in terms of the crystal-field (CF) model applied to the Mn^{2+} site, a number of problems remain. Application of advanced molecular quantum-chemical methodologies can provide quantitative analysis and resolution of several of them. In this paper we consider further[2] the electronic structure and absorption spectrum of the MnS_4^{6-} cluster, which is often assumed to be a realistic model of the Mn^{2+} deep center in the prototypical $Zn_{1-x}Mn_xS$ crystal.

A. Observed optical-absorption spectra

The time-independent features of the spectroscopy of these materials show clearly a considerable separation between the band properties of the host and the localized character of Mn^{2+} in its ground and lower excited states. The positions of absorptions ascribed to Mn^{2+} (see Table I) are at most slightly dependent upon temperature and concentration of Mn^{2+} and weakly dependent upon the particular host system.[1] This division has long been assumed with the sulfides; most recently and conclusively it has been established also for the Zn or Cd with Se or Te systems by the magnetoreflectance and photoconductivity experiments of Lee, Ramdas, and Aggarwal.[3]

While considerable structure in the Mn^{2+} bands has been observed in ZnS:Mn and ZnSe:Mn below 3.7 eV, little if any has been seen for the others.

Similarities in positions of absorption bands suggest that other characteristics of the spectra may also be similar. Observations made on the heavier II-VI systems will later be correlated with calculated properties of MnS_4 in the discussions following.

B. Geometry at the Mn^{2+} site

X-ray structural investigations of $Zn_{1-x}Mn_xS$ solid solutions, as functions of temperature and x (Ref. 4) show that both cations retain four nearest S neighbors in near-T_d symmetry in both zinc-blende (ZB) and wurtzite

structure. The *mean* anion-cation distance varies from 2.345 Å ($x=0$) to 2.384 Å ($x=0.45$); in ZB β-MnS it is 2.43 Å and in wurtzite MnS it is 2.41 Å. The *actual* Mn-S geometry in the solid solution phase is not certain, however. Recent extended x-ray-absorption fine structure (EXAFS) studies on $Cd_{1-x}Mn_xTe$ (Refs. 5 and 6) and $Zn_{1-x}Mn_x$ Se (Ref. 7), for example, indicate that individual pairs of anion-cation distances remain nearly constant (at their pure phase values) independent of x. Results on the Zn-Mn-S system have not been reported, but would likely be similar.

C. Semiempirical CF analyses of the absorption spectrum

Crystal-field diagrams for the d^5 configuration (see Fig. 1) have been employed to assign the various transitions observed. Diagrams based upon free-ion values for the relevant parameters (atomic excitation energies and Racah B and C parameters)[8] have several quantitative shortcomings, however. To fit the absolute position of the lowest transition requires a CF splitting parameter $Dq \sim 1000$ cm^{-1}, but to encompass five or six transitions within the observed 7000-cm^{-1}-wide interval requires $Dq \sim 300$ cm^{-1}. In either range, the lowest three bands are identified as ${}^6A_1 \rightarrow {}^4T_1, {}^4T_2, {}^4E + {}^4A_1$. Assignment of the next three is either ${}^6A_1 \rightarrow {}^4T_1, {}^4E, {}^4T_2$ or ${}^6A_1 \rightarrow {}^4T_2, {}^4E, {}^4T_1$. (Note also in simple CF theory that the lower ${}^4E_g$ and ${}^4A_1$ are degenerate and, with ${}^4A_2$, independent of Dq.)

Thus, to fit CF diagrams accurately to experimental data has required free adjustment of all parameters (Dq, B, and C, plus a variety of others). In systems exhibiting only a few bands, the CF fits are therefore quite arbitrary.

Excerpts from the history of attempts to fit the ZnS:Mn^{2+} data are given in Table II. A hint of the difficulties is shown by similar attempts to fit just the ${}^6S \rightarrow {}^4G, {}^4P, {}^4D, {}^4F$ excitation energies of the free Mn^{2+} ion.

Gumlich *et al.*[9] fit the absorption maxima with $Dq = 500$ cm^{-1} and up to 35% reduction in free-ion Racah parameters, which, incidentally, produces an inversion of the effective atomic ${}^4P$ and ${}^4D$ levels. They identify the fourth band as excitation to ${}^4T_2({}^4D)$ rather than to ${}^4T_1({}^4P)$; the fitted value, however, is too high by about 2000 cm^{-1}.

Curie, Barthou, and Canny[10] investigated in considerable detail the effects of "covalency" upon the values of the relevant parameters, including the Trees and seniority parameters λ and β, respectively. Following Koide and Pryce,[11] they noted that the $3d$ atomic orbitals (AO's) may become delocalized through the formation of e- and t-type molecular orbitals (MO's), with resulting changes

TABLE I. Positions of absorption bands in $A^{II}_{1-x}Mn_xC^{VI}$ systems (energies in eV), with assignments given.

Host	Band edge	Positions of Mn^{2+} bands and assignments: ${}^4T_1$	${}^4T_2$	${}^4E, {}^4A_1$	${}^4T_1$ or ${}^4T_2$ or ${}^2T_2$	${}^4E$	Comments	Footnote
ZnS	3.8[a]	2.218	2.440	2.633	2.812	3.136	0 phonon	f
		2.34	2.49	2.67	2.89	3.15+3.19	maxima	
CdS	>2.5[b]	2.308 (0 ph)	2.58	2.72			transmission	b
		2.44 (max)						
ZnSe	>2.8[c]	2.235	2.430	2.617			0 ph	g,h
		2.38–2.42	2.51–2.54	2.68–2.70	2.93±		max ($0.23 < x < 0.5$)	i
CdSe	>1.8[d]	2.3→	2.4				broad shoulder	j
ZnTe	>2.4[e]	2.33	2.40	2.605	2.745		$x \sim 0.6$	k
CdTe	>1.6[a]	2.18→	2.43	2.63				

[a] *Landolt-Börnstein, Physics of II–VI and I–VII Compounds, Semimagnetic Semiconductors,* edited by O. Madelung (Springer-Verlag, Berlin, 1982), Vol. III/17b.

[b] M. Ikeda, K. Itoh, and H. Sato, J. Phys. Soc. Jpn. **25**, 455 (1968).

[c] R. B. Bylsma, W. M. Becker, J. Kossut, U. Debska, and D. Yoder-Short, Phys. Rev. B **33**, 8207 (1986). [For $0 < x < 0.1$, the free exciton energy decreases with x; beyond $x = 0.05$ it increases. A. Twardowski, T. Dietl, and M. Demianiuk, Solid State Commun. **48**, 845 (1983).]

[d] J. Antoszewski and E. K. Pecold, Solid State Commun. **34**, 733 (1980).

[e] P. Swiderski, A. Twardowski, and I. Glass, Polska Akad. Nauk **6**, 436 (1983).

[f] Data are compiled in Ref. 10. The band whose maximum is at 3.19 eV consists of two bands, at 3.15 and 3.19 eV, according to A. Mehra, J. Electrochem. Soc. **118**, 136 (1971). The 0-phonon lines were determined by D. Langer and S. Ibuki, Phys. Rev. **138**, A809 (1965).

[g] D. Langer and H. J. Richter, Phys. Rev. **146**, 554 (1966). ($x < 0.001$.)

[h] G. Jones and J. Woods, J. Phys. D **6**, 1640 (1973). ($x < 0.01$.)

[i] W. M. Becker, in *Semiconductors and Semimetals,* edited by J. K. Furdyna and J. Kossut (Academic, New York, 1988), p. 35.

[j] J. E. Morales-Toro, W. M. Becker, and U. Debska, Phys. Rev. B **32**, 5202 (1985).

[k] J. E. Morales-Toro, W. M. Becker, B. I. Wang, U. Debska, and J. W. Richardson, Solid State Commun. **52**, 41 (1984).

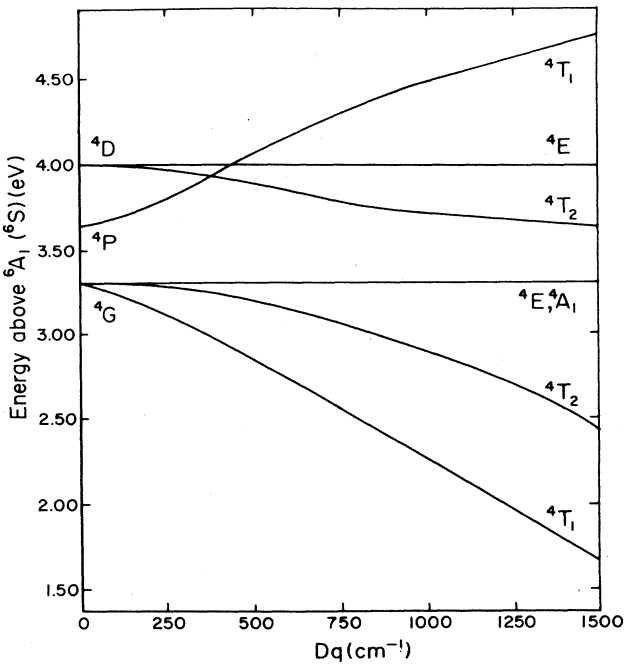

FIG. 1. Crystal-field energy-level diagram for lower excited states of Mn^{2+}, which are seen in ZnS, based upon free-ion parameters.

in the orbitals,

$$3de_{AO} \rightarrow N_e(3de - \mu_e\chi_e)_{MO} ,$$
$$3dt_{AO} \rightarrow N_t(3dt - \mu_t\chi_t)_{MO} , \quad (1.1)$$

in which χ_e and χ_t are appropriate linear combinations of AO's on the nearest anions (e.g., S) and μ_e and μ_t are small coefficients. Thereby the cluster *d-d* electrostatic interaction integrals become free-ion *A*, *B*, and *C* parameters scaled down by appropriate products of N_e^2 and N_t^2. They examined spectral fits using various combinations of *Dq* values and *d* character in the MO's. (See Table II.) They also concluded that the effective atomic ^4D level lies below ^4P, so that the fourth band in the ZnS:Mn^{2+} spectrum is $^4T_2(^4D)$, not $^4T_1(^4P)$, unless *Dq* should become less than 300 cm^{-1}. All their effective quartet levels are depressed below free-ion values by 6000–8000 cm^{-1} by the presumed orbital covalency effects.

These authors also showed a removal of the degeneracy of the $^4A_1$ and ^4E levels arising from ^4G. From calculations with, e.g., $\varepsilon = (1 - N_t^2/N_e^2) < 1$ (i.e., with more delocalization assumed in the σ-bonding *t* MO's, than in the π-bonding *e* MO's), the ^4E level may lie as much as 1500 cm^{-1} below $^4A_1$.

Recently, Fazzio, Caldas, and Zunger[12] parametrized the lower transitions for a series of ZnS:M^{2+}, ZnSe:M^{2+}, and GaP:M^{2+} compounds, using a simpler version of the procedures of Curie *et al.* For ZnS:Mn^{2+} and

TABLE II. Parameters for crystal-field fits to sextet-quartet transitions in MnS_4^{6-} (energies in cm^{-1}).

System	*Dq*	*B*	*C*	Other[a]	Reference
Free Mn^{2+}		960	3325		8
		950	3280		b
		960	3210		9
		918	3273	$\lambda=65$, $\beta=-131$	10
		914	3274	$\lambda=72$, $\beta=-127$	10[c]
ZnS:Mn^{2+}	500	610	3100		9
to max	375	716	2553	$\lambda=65$, $x=0.78$, $\varepsilon=0$	10
to 0 ph	495				
to max	325	802	2861	$\lambda=65$, $x=0.874$, $\varepsilon=0.1$	10
to 0 ph	440				
to max	315	918	3273	$\lambda=65$, $x=1$, $\varepsilon=0.2$	10
to 0 ph	422				
	420	730	2880		13
ZnSe:Mn^{2+}	405	740	2740		d

[a]λ is the Racah-Trees parameter and β is the seniority number. $x = N_e^4$, $\varepsilon = 1 - N_t^2/N_e^2$, $B = xB_0$, and $C = xC_0$; B_0 and C_0 are the free-ion values; N_e and N_t are the normalization factors for the appropriate 3*d* AO's in the *e*- and *t*-type MO's of the MnS_4 cluster.

[b]J. W. Stout, J. Chem. Phys. **31**, 709 (1959).

[c]Includes a fit also to the $^6S \rightarrow {}^2I$ transition.

[d]R. Parrot, C. Naud, C. Porte, D. Fournier, A. C. Boccara, and J. C. Rivoul, Phys. Rev. B **17**, 1057 (1978).

ZnSe:Mn^{2+} their conclusions are similar. In particular, their N_e^2 and N_t^2 equal 0.983 and 0.967, respectively; they conclude that $^4A_1$ is always higher than $b\,^4E$, by ~ 390 cm^{-1} in this system.

Unfortunately, there appears to be no clear experimental estimate of the separation between the $^4A_1$ and ^4E levels. In a careful study of the ^4E region in ZnS:Mn^{2+}, Parrot and Blanchard[13] explained the observed structure in terms of small interactions with ^4E levels only. Furthermore, their theoretical analysis also indicates that the $^6A_1 \rightarrow {}^4A_1$ transition is strongly forbidden. The accurate positioning of these levels is also obscured by spin-orbit interactions.

A related issue is the dependence of the $^4A_1$ and $a\,^4E$ excitation energy upon Dq or R, not found in basic CF theory. Ves *et al.*[14] established this variation in the spectrum of $Zn_{1-x}Mn_xSe$ under hydrostatic pressure and related it to changes in the B parameter with R.

Some of these effects were anticipated in connection with theoretical studies of the cubic MnF_6^{4-} system by Lohr[15] and analyzed in detail by Flórez, Sejio, and Pueyo,[16] who found crossing of $^4A_1$ and $a\,^4E$ at larger Mn-F distances.

As a further refinement of fits to empirical spectra, Parrot *et al.*[17] and Boulanger and Parrot[18] have used the semiempirical angular overlap model to examine possible Jahn-Teller distortions in the excited states of Mn^{2+} in ZnS and ZnSe.

D. Relevant nonempirical calculations

Until the present studies were undertaken[19] previous calculations of Mn-chalcogenide spectra have been at least partially semiempirical. The works of Zunger *et al.* (surveyed in Ref. 1, pp. 392ff) on a variety of metal ions in II-VI, III-V, Si, and Ga-P hosts begin with a first-principles calculation of self-consistent, mean-field electronic charge distributions using a quasiband crystal-field Green's-function approach involving pseudopotentials of the host and the local-density approximation of interelectronic Coulomb and exchange interactions. Upon this basis, however, it is still necessary to invoke parametrized fits to observed spectra, as noted above.

The present work evolves from a large body of first-principles spectral calculations of transition-metal cluster systems by many research groups. Only a few, most relevant are cited (Refs. 20–22; see also references in Ref. 1). They have been largely limited to self-consistent-field (SCF) MO calculations of d^n ground and excited states, occasionally combined with configuration interaction (CI) among those states and with correction for other intra-d-shell correlation effects.

Apart from developing methodology, these many works produced a reasonably good interpretation of observed electronic properties but also quantitatively defined certain inadequacies in the models used. They also indicated considerably smaller degrees of electronic delocalization than obtained from purely empirical CF fitting of spectra.

Calculations based upon the $X\alpha$ local-density approximation, introduced by Johnson and Smith,[23] have tended to produce greater delocalization. While some correlation effects are included, the method suffers disadvantages in interpretation and in application to the d multiplets. Electronic self-interaction is not exactly canceled, electronic states are not precisely described, and it is not possible to characterize exactly what types to correlation effects are included. The method does have many conceptual advantages and simplicities, however, and corrective measures are under study.[24–26]

Relevance of charge-transfer character in the d^n states were first indicated by Hubbard, Rimmer, and Hopgood[27] as part of a proposed valence-bond model. In the CuF_6^{4-} cluster, Shaskin and Goddard[28] added several hundred other states to the d states, obtained from SCF calculations, as a basis for CI calculations of the spectrum. The other states were limited to those of the pure d and CT calculations, plus single excitations from them. These terms significantly increased the separations between calculated visible transitions to good agreement with experiment.

The $CuCl_4$ and NiO_6 clusters have also been studied recently, with even greater numbers and varieties of charge-transfer–based states included by CI with the d^n states.[19,29,30] In those cases also, limiting to correlation effects described only by d^n states produced optical transition energies that were too small, as found, for example, in $CuCl_4^{2-}$ and NiO_6^{10-}. In these works, both single and some types of double excitations were constructed from the d^n and CT configurations; categories of such states were defined and identified with distinct types of electron correlation effects being included. In the d^9 $CuCl_4$ system, delocalization and splitting of the ^2E and $^2T_2$ states are thereby increased toward closer agreement with experiment.[30] Similar improvements were also obtained for the spectrum of NiO_6^{10-} (Ref. 30) and for estimates of d ionization energies, the Mott-Hubbard gap and the charge-transfer gap in NiO.[30]

The approach used here for the MnS_4^{6-} cluster in ZnS is close to that used for the $CuCl_4$ cluster. A large Gaussian basis provides appropriate SCF MO's and energies. Electron correlation effects are then introduced by CI in stages. The lower-level results correspond more closely to the still widely used ligand-field approximation; they are analyzed to assess quantitatively the parameters of that model and to document their physical deficiencies. The higher-level results include CI with CT-based cluster states, though less extensive than in $CuCl_4$ and NiO_6 because of their greater proliferation in MnS_4. Large improvements are also obtained here. These correlation effects are analyzed to identify physical features of the metal-ligand interaction beyond the scope of the present ligand-field model.

II. THEORETICAL MODEL AND METHODOLOGY

Results presented are based upon the assumption that the features of optical absorption below the band edge are primarily determined by the lower-energy states of electronically isolated MnS_4^{6-} clusters, each perturbed at most by the electrostatic field from the rest of the crystal.

Weaker effects, interactions such as those with band states of the host and between adjacent Mn-Mn pairs, may subsequently be treated in terms of the localized states thus determined.

The methodology begins with determining sets of one-electron orbital functions, self-consistent-field (SCF) MO's, for the ground and other states of the systems. These SCF MO's, in turn, are the basis for incorporating several types of electron correlation essential for accurate assessment of bonding and electronic excitation energies in these systems.

A. Hamiltonian and electronic states

Calculations are reported here for tetrahedral MnS_4 at three Mn-S distances, 4.2917, 4.5917 (β-MnS), and 4.8917 a.u. (2.27, 2.43, and 2.59 Å, respectively) which span the region of interest. A fixed external electrostatic potential, V(ext), is constructed to represent a zinc-blende environment of $+2$ and -2 point charges with R(Zn-S)=4.426 a.u. (2.34 Å). V(ext) is nearly constant in the region of the MnS_4 cluster. Since the results presented below are quite insensitive to its presence and since $+2$ and -2 are very close to the final Mn and S net charges calculated here for MnS_4^{6-}, no attempt was made to refine V(ext). The nonrelativistic Born-Oppenheimer Hamiltonian, $\hat{H}$, thus includes kinetic energies and the potential energies of interaction among the five nuclei and 95 electrons of the cluster and, optionally, V(ext).

MO's calculated for the cluster are named according to the a_1, e, t_1, and t_2 representations of the T_d group; within each symmetry type they are sequentially numbered in order of increasing orbital energy. Each may be characterized according to its major atomic contributions as follows:

(a) inner shells $1s;2s;2p;3s;3p$ of Mn$\rightarrow 1a_1;3a_1;2t_2;6a_1;6t_2$;

(b) inner shells $1s;2s;2p;3s$ of the four S$\rightarrow 2a_1;1t_2;4a_1,3t_2;5a_1,1e,1t_1,4t_2,5t_2;7a_1,7t_2$;

(c) Mn-S bonding (mainly S $3p$ in character) $\rightarrow 8a_1,2e,8t_2,9t_2$;

(d) nonbonding ($3p$ localized on the S)$\rightarrow 2t_1$;

(e) Mn-S antibonding (mainly Mn $3d$ in character)$\rightarrow 3e,10t_2$.

[For convenience, the doubly degenerate $3e$ and triply degenerate $10t_2$ MO's will simply be labeled e (with components θ and ε) and t (with components ξ,η,ζ), respectively.]

Also produced by the SCF procedure are sets of *virtual* MO's (not *formally* occupied in the states of interest). For later reference they are divided into three categories according to their spatial distribution:

(f) orthogonal complements to the core MO's in categories (a) and (b), which are large only in the regions of the inner-shell MO's;

(g) orthogonal complements to $2t_1$ in category (d), which are large only in the regions of the four S atoms;

(h) orthogonal complements to Mn-S MO's of categories (c) and (e). These span the regions of Mn-S overlap.

Electronic states of interest here derive mainly from configurations in which all Mo's of categories (a), (b), (c), and (d) are occupied by 90 electrons and the open-shell e and t MO's [category (e)] are variously occupied by five:

$$[\text{closed shells}]^{90}e^x t^y, \quad (x,y)=(1,4),(2,3),(3,2)\ . \tag{2.1}$$

For each (pure) configuration, couplings among unpaired electrons produce one or more wave functions [each called a pure configuration-state function (CSF)] of particular spin and space symmetry. CSF's of the pair configurations (2.1) will be indicated by $|iS\Gamma\rangle$, where S is the total spin quantum number, Γ designates the orbital symmetry representation, and i is a sequence number. (Note that designations of spin and spatial degeneracies are suppressed.) They include[31]

$(x,y)=(1,4)$ with $iS\Gamma \sim 1\,^4T_1,\ 1\,^4T_2$,

$(x,y)=(2,3)$ with $iS\Gamma \sim 1\,^6A_1,\ 1\,^4A_1,\ 1\,^4A_2,\ 2\,^4T_1,\ 2\,^4T_2,\ 1\,^4E,\ 2\,^4E$,

$(x,y)=(3,2)$ with $iS\Gamma \sim 3\,^4T_1,\ 3\,^4T_2$,

plus a number of doublet states not considered here.

CSF's of higher energy are created by transferring one or more electrons from MO's occupied in configurations (2.1) to available open-shell and virtual MO's. Included in the present work are three types of one-electron transfers between various categories:

$$(c)\rightarrow(e)\ , \tag{2.2}$$

S-Mn charge-transfer promotions, and

$$(c)\rightarrow(h)\ \text{ and }\ (e)\rightarrow(h)\ , \tag{2.3}$$

"relaxation" promotions. Note that MO's in categories (a),(b),(d) are regarded as frozen orbitals; they and (for reasons of computation limitations on size) some virtual MO's (f),(g), have been omitted in constructing these high-energy CSF's.

B. SCF calculations

All MO's for the cluster are represented by large Gaussian bases: for Mn, the (14,9,5) set of Wachters[32] plus diffuse p and d functions;[33] for S, the (10,6) set of Roos and Siegbahn.[34]

Open-shell self-consistent-field (SCF) calculations using spin- and symmetry-restricted orbitals were performed for the T_d point-group cluster at the three Mn-S distances, using the SYMOL program at the University of Groningen.[35] Results were obtained for states of the pure $e^x t^y$ configurations and also for a hypothetical state, called $\overline{H}$, whose energy is the average of the 25 sextet and quartet levels and which has the advantage of giving a good set of MO's for all configurations (2.1).

C. Excitation energies and inclusion of electron correlation effects

Including effects of electron correlation is essential for accuracy in calculating excitation energies. Among the various types of effects, three appear especially important and are incorporated here. These are as follows: (a) Atomic differential correlation effects for the $3d^5$ states of the free Mn^{2+} ion; these are introduced by the correlation-energy–correction (CEC) method.[22] (b) Additional correlations among the $3d$ electrons accompanying the reduction to the lower symmetry of the cluster; these are introduced by the CI method, wherein a better approximation to each state is obtained by variationally optimizing a linear combination of CSF's belonging to the main configurations (2.1). (This procedure is here termed LF-CI and is formally equivalent to the CF scheme based upon the strong-field-coupling scheme.[31]) (c) As established by parallel studies on the $CuCl_4$ and NiO_6 systems[2,30] and by this work, further CI, specific to the particular metal-ligand combination and here called RCT-CI, is important. Details are given in the following two sections.

1. LF-CI and CEC

LF-CI and CEC are conveniently considered together. In the original formulation,[22] LF-CI wave functions, called $\Phi(nS\Gamma)$, are expressed by

$$\Phi(nS\Gamma)=\sum C_{n,iS\Gamma}|iS\Gamma\rangle \ , \tag{2.4}$$

where the $C_{n,iS\Gamma}$ are variational coefficients, n is a sequence symbol $(a,b,\ldots)$, and each sum runs over all CSF's of the same $S\Gamma$.

The Hamiltonian for the MnS_4 cluster is represented at this level by the matrix $\underline{H}$ on the $|iS\Gamma\rangle$ basis:

$$\underline{H}=\underline{H}_0+\underline{H}_{\text{LF-CI}}+\underline{H}_{\text{CEC}} \ . \tag{2.5}$$

$\underline{H}$ is block diagonal according to values of $S\Gamma$. The nonzero elements

$$(\underline{H}_0+\underline{H}_{\text{LF-CI}})_{i'S\Gamma,iS\Gamma}=\langle i'S\Gamma|\hat{H}|iS\Gamma\rangle \tag{2.6}$$

may then be evaluated in terms of open-shell SCF orbital energies, nine unique J and K integrals and one other integral[36] among the e and t MO's, using standard procedures.[37,38] $\underline{H}_0$ and $\underline{H}_{\text{LF-CI}}$ are the diagonal and off-diagonal parts of this matrix, respectively.

The CEC required here are first defined as the differential correlation-energy corrections with respect to the ground state, in the free Mn^{2+} ion,

$$\Delta E_{\text{CEC}}(SL)=\Delta E_{\text{obs}}(SL)-\Delta E_{\text{SCF}}(SL) \ , \tag{2.7}$$

where $SL={}^4G$, ${}^4P$, ${}^4D$, and ${}^4F$; ΔE_{obs} and ΔE_{SCF} are the excitation energies relative to the ground state, $SL={}^6S$, observed and calculated from SCF treatment of the free ion, and $\Delta E_{\text{CEC}}({}^6S_1)\equiv 0$. The CEC is represented on the free-ion basis $|SL\rangle_0$ by a diagonal matrix

$$\langle S'L'|\hat{V}|SL\rangle_0=\Delta E_{\text{CEC}}(SL)\delta_{SS'}\delta_{LL'} \ . \tag{2.8}$$

The free-ion states $|SL\rangle_0$ are represented as linear combinations of states of the free-ion strong-field configurations, $|iS\Gamma\rangle_0$,

$$|SL\rangle_0=\sum_{iS\Gamma}|iS\Gamma\rangle_0\langle iS\Gamma|SL\rangle_0 \ . \tag{2.9}$$

The coefficients $\langle iS\Gamma|SL\rangle_0$ are fixed by symmetry.[39] The CEC matrix of Eq. (2.8) is then transformed to the matrix $\underline{H}_{\text{CEC}}$ with nonzero elements

$$\langle i'|S\Gamma|\hat{V}|iS\Gamma\rangle_0 = \langle i'S'\Gamma'|S'L'\rangle_0\langle S'L'|\hat{V}|SL\rangle_0\langle SL|is\Gamma\rangle_0 \ . \tag{2.10}$$

This matrix may be formed with the same structure as the LF-CI matrix, so that Eq. (2.5) may follow.

The diagonal elements of $\underline{H}_0$ are the (first-order) energies, $E_0(iS\Gamma)$, of pure-configurational states, $|iS\Gamma\rangle$. Eigenvalues and eigenvectors of $(\underline{H}_0+\underline{H}_{\text{LF-CI}})$ and of $\underline{H}=(\underline{H}_0+\underline{H}_{\text{LF-CI}}+\underline{H}_{\text{CEC}})$ show the effects of including LF-CI and CEC improvements to the calculation. Excitation energies may then be calculated from the latter two sets of eigenvalues, respectively:

$$\Delta E(\text{LF-CI},nS\Gamma)=E(\text{LF-CI},nS\Gamma)-E(\text{LF-CI},{}^6A_1) \ , \tag{2.11}$$

$$\Delta E(\text{LF-CI+CEC},nS\Gamma)=E(\text{LF-CI+CEC},nS\Gamma) - E(\text{LF-CI+CEC},{}^6A_1) \ .$$

When using SCF MO's from the hypothetical $\bar{H}$ state and especially in later work on distorted clusters in which orbital degeneracies are lifted, generalization of Eq. (2.6) is necessary. Since $\hat{H}$ is spin independent, it is sufficient to consider only the $M_s=+\frac{3}{2}$ components of each sextet and quartet level of the system. Specific CSF's, $|iS\Gamma\frac{3}{2}\rangle$, for these 25 states can be written as linear combinations of 25 single determinantal functions,

$$|\bar{k}\rangle=C_{\bar{k}}^{\dagger}C_lD_0 \ ,$$

where k and l range over the five open-shell e and t MO's $(\theta,\varepsilon,\xi,\eta,\zeta)$; D_0 is the $M_s=\frac{5}{2}$ ${}^6A_1$ ground-state determinantal function:

$$D_0=|(\text{closed shells})\ \theta\varepsilon\xi\eta\zeta\rangle$$

and $C_{\bar{k}}^{\dagger}C_l$ replaces the lth MO (with α spin) by the kth MO with β spin. On this alternative basis Eq. (2.6) becomes

$$(\underline{H}_0+\underline{H}_{\text{LF-CI}})_{\bar{k},l',\bar{k}l}=\langle \bar{k}l'|\hat{H}|\bar{k}l\rangle \tag{2.6'}$$

and Eq. (2.10) becomes

$$\langle \bar{k}\,l'|\hat{V}|\bar{k}l\rangle=\langle \bar{k}\,l'|S'L'\rangle_0\langle S'L'|\hat{V}|SL\rangle\langle SL|\bar{k}l\rangle \ . \tag{2.10'}$$

Eigenvalues of $(\underline{H}_0+\underline{H}_{\text{LF-CI}})$ and of $\underline{H}$, of course, have the same interpretation as before.

2. RCT-CI and alternative treatment of CEC

The extent of electron correlation effects was further examined by adding many more CSF's to the simpler LF-CI wave functions, Eq. (2.4). Because of limitations on computer time and storage, these calculations were restricted to the β-MnS distance (2.43 Å) and only those types of additional CSF's were included which were found to be significant in prior, although otherwise parallel, calculations [termed first-order configuration-interaction (FOCI)] on the $CuCl_4^{2-}$ and NiO_6^{10-} clusters, having only one and two unpaired electrons, respectively.[30,40] The relaxed–charge-transfer-state configuration-interaction (RCT-CI) wave functions are linear combinations of CSF's from configurations not only of type (2.1) but also of those higher-energy types (2.2) and (2.3) described in Sec. II A.

The additional CSF's are obtained as follows. First, for each symmetry ($S\Gamma$), a so-called reference set is constructed, which includes the (2.1)-type CSF's plus all other CSF's of the same $S\Gamma$ that belong to those configurations differing from a (2.1) configuration by a single-electron (c)→(e) charge-transfer promotion. The remaining CSF's are then constructed by allowing all further single-electron (c)→(h) and (e)→(h) promotions with respect to all CSF's in the reference set. In general this procedure is called multireference singles CI;[40] here it will be termed RCT-CI, since the physical effect is to include relaxed CT states.[30]

It should be noted that these additional CSF's are semi-internal, double replacements with respect to the d^n states. However, they do not contribute to the *atomic* correlation energies; instead, they provide for *molecular* correlation effects. Including the CT CSF's alters the extent of net S-Mn electron transfer. Including CSF's with one electron in the (h) set in effect allows for electronic polarization and relaxation in the CT states. Through second-order coupling *via* these additional CSF's, the CT CSF's are mixed into the wave function.

The matrix of $\hat{H}$ on this augmented basis is automatically generated and the lowest required eigenvalues and eigenvectors were obtained from a general CI program package developed by Hegarty.[41] This program was designed to handle molecules having Abelian point-group symmetry. Therefore, the present calculation was done using the D_2 subgroup of T_d; the higher symmetry was enforced, however, by using the T_d-symmetry adapted integrals output from the SCF calculation.[42]

In principle, an appropriately constructed $\underline{H}_{\text{CEC}}$ matrix also should be added to the CT-CI matrices. For practical reasons, however, this was not done and the CEC-type corrections were added to excitation energies, $\Delta E(\text{RCT-CI},nS\Gamma)$, calculated from eigenvalues of the CT-CI matrices. Each relevant RCT-CI wave function, $\Psi(nS\Gamma)$, is dominated by the LF-CI type contributions, $\Phi(nS\Gamma)$:

$$\Psi(nS\Gamma)=\lambda_{nS\Gamma}\Phi(nS\Gamma)+\text{other CSF's}\ , \tag{2.12}$$

where $\lambda_{nS\Gamma}\sim 1$. A *molecular* CEC may be defined for each state of the cluster by

$$\Delta E_{\text{CEC}}(nS\Gamma)=\Delta E(\text{LF-CI}+\text{CEC},nS\Gamma)-\Delta E(\text{LF-CI},nS\Gamma)\ , \tag{2.13}$$

using Eqs. (2.11). The excitation energies corresponding to the level using Eqs. (2.11). The excitation energies corresponding to the level CT-CI+CEC are now obtained from

$$\Delta E(\text{RCT-CI}+\text{CEC},nS\Gamma)=\Delta E(\text{RCT-CI},nS\Gamma)+\lambda^2_{nS\Gamma}\Delta E_{\text{CEC}}(nS\Gamma)\ . \tag{2.14}$$

This last equation assumes that all $\lambda^2_{nS\Gamma}$ are equal. In fact, most are found to differ from 0.95 by less than ± 0.03 and thus the resulting error is less than ± 0.03 eV.

III. RESULTS

Free-ion results are discussed first, since they determine the CEC elements and the calculated binding energy of the cluster. Cluster SCF orbital characteristics are then examined relative to empirical CF fittings and to orbital relaxation effects accompanying excitation, ionization, and electron attachment. Analysis of spectral results begins at the LF-CI+CEC level, since these more extensive calculations already reveal much about the nature of the excited states. Finally, the best spectral results, obtained from the RCT-CI+CEC level, establish the major effects due to charge-transfer, cluster-specific electron correlation in this type of system.

A. Energies of Mn^{2+} and S^{2-} ions

Using the respective portions of the MnS_4 basis, restricted atomic SCF calculations were made upon the sextet and quartet states of Mn^{2+} and the ^1S state of S^{2-}. Calculated total energies are $-1149.033\,65$ and $-397.055\,17$ a.u. for $Mn^{2+}(^6S)$ and S^{2-}, respectively. See Table III.

Energies of excitation calculated from independent SCF's on the Mn^{2+} states, ΔE_{SCF}, are slightly smaller (by 0.03–0.08 eV) than those calculated using fixed values of the *d-d* interaction integrals obtained from the SCF of the ^6S ground state. These several differences indicate the extent of differential electronic relaxation of the AO's accompanying excitations within the $3d^5$ manifold.

Each element required for the $\Delta E_{\text{CEC}}(SL)$ matrix, Eq. (2.7), is the difference between ΔE (calculated from the ^6S SCF) and ΔE_{expt}. Clearly seen are the familiar differing extents of electron correlation effects in each quartet level.

The *d-d* interaction integrals from the ^6S SCF may be used to determine SCF values of Racah parameters: $A=22.0613$ eV, $B=0.1415$ eV (1141 cm^{-1}), and $C=0.5245$ eV (4231 cm^{-1}). These values of B and C are about 25% greater than the empirically fit values in Table II. The empirical B and C values are forced to contain significant amounts of differential correlation energies as well as smaller amounts from orbital relaxation; these are two electronic properties not properly represented by the fixed pure-configurational orbital model upon which the fitting procedure is based. This feature becomes even

TABLE III. Excitation energies and $\Delta E_{CEC}(SL)$ for Mn^{2+} (in eV).

Excitation $^6S\rightarrow$	ΔE_{SCF}	ΔE from ^6S SCF	ΔE (expt.)[a]	$\Delta E_{CEC}(SL)$[b]
^4G	4.009	4.037	3.328	−0.709
^4P	4.622	4.662	3.620	−1.042
^4D	4.968	5.028	4.011	−1.017
^4F	6.705	6.784	5.408	−1.376
^2I		5.84	4.86	−0.98

[a]C. H. Corliss and J. Sugar, J. Phys. Chem. Ref. Data **6**, 1253 (1977). Values given result from $(2J+1)$-weighted averaging of observed levels, approximately to eliminate spin-orbit energies.
[b]Using ΔE's from SCF on ^6S.

more important when interpreting the spectrum of the cluster.

B. Characteristics of SCF MO's and energies

1. Delocalization of 3d electrons

The large and flexible Gaussian basis used makes difficult a direct quantitative measure of electronic delocalization in the spectrally and magnetically important e and t MO's. The usual Mulliken population analysis yields a formal configuration of $3de^{1.90}3dt^{3.08}4s^{0.37}4p^{0.61}$ for Mn in the cluster at 2.43 Å. Since the diffuse 4s and 4p AO's are mostly in the region of the ligands, Mn effectively has a net charge of +2.02. The same analysis gives a delocalization of 0.4% and 2.8% in the de and dt MO's, respectively. A more useful alternative is to assess the orbital reduction of "d-d" repulsion integrals from free-ion values, as described in Sec. I C. Table IV defines and displays values of six of the ten independent integrals obtained from the SCF calculation on ^6S Mn^{2+} and the percent reductions obtained from SCF calculations on the $^6A_1$ and $\bar{H}$ states of the cluster at the three distances. These numbers portray several interesting aspects of the Mn-S covalency.

(a) Reductions in the ground state are all between 2.3%

TABLE IV. SCF orbital characteristics of MnS_4.

Quantity[a]	Integral value (free Mn^{2+} ^6S) (in a.u.)	$MnS_4(^6A_1)$ without V(ext) (R = 2.43 Å)	Percent reduction from free-ion values (in a.u.)[c]: $MnS_4(^6A_1)$ with V(ext) R(Å)= 2.27	2.43	2.59	$MnS_4(\bar{H})$ with V(ext) R(Å)= 2.27	2.43	2.59
$\bar{J}(tt)$	0.842 89	4.15	5.50	3.97	3.03	8.14	6.29	5.14
$\bar{K}(tt)$	0.319 71	4.24	5.62	4.06	3.11	8.36	6.46	5.29
$\bar{J}(et)$	0.830 04	3.60	4.58	3.41	2.78	6.89	5.45	4.53
$\bar{K}(et)$	0.029 68	4.61	6.00	4.46	3.47	9.16	7.26	6.04
$\bar{J}(ee)$	0.849 31	3.07	3.68	2.87	2.31	5.68	4.66	3.97
$\bar{K}(ee)$	0.464 73	3.13	3.76	2.93	2.36	5.82	4.77	4.07
$\varepsilon^0(e)$		+0.4896	−0.5486	−0.5971	−0.6462	−0.4828	−0.5337	−0.5842
$\varepsilon^0(t)$		+0.5046	−0.5240	−0.5802	−0.6341	−0.4598	−0.5173	−0.5721
			From $\bar{I}=\bar{J}$					
N_e^2		0.9845	0.9814	0.9855	0.9884	0.9712	0.9764	0.9799
N_t^2		0.9790	0.9721	0.9799	0.9847	0.9584	0.9680	0.9740
$100(1-N_e^2N_t^2)$[b]		3.61	4.59	3.43	2.67	6.92	5.48	4.56
			From $\bar{I}=\bar{K}$					
N_e^2		0.9810	0.9812	0.9852	0.9881	0.9705	0.9758	0.9794
N_t^2		0.9715	0.9715	0.9795	0.9843	0.9573	0.9672	0.9732
$100(1-N_e^2N_t^2)$[b]		4.69	4.68	3.50	2.74	7.09	5.62	4.68

[a]$I=J$ or K; $\bar{I}(\mu,\nu)$ is the average interaction, Coulombic or exchange, between electrons $\mu,\nu=e,t$. $\bar{I}(ee)=[I(\theta\theta)+I(\theta e)]/2$, $\bar{I}(tt)=[I(\zeta\xi)+I(\zeta\eta)+I(\xi\xi)]/3$, and $\bar{I}(et)=[I(\theta\xi)+I(\varepsilon\xi)]/2$, where $\theta,\varepsilon,\xi,\eta,\zeta$ are specific MO's of the e,t types. $\varepsilon^0(e)$ and $\varepsilon^0(t)$ are the open-shell orbital energies of the "3d" MO's. N_e^2 and N_t^2 are defined in the text surrounding Eqs. (3.1)–(3.3).
[b]Percent reduction is $100[1-I(\mu\nu)/I_0(\mu\nu)]$.
[c]These values related to estimates of $\bar{K}(et)$, using Eqs. (3.3), and are to be compared to the actual reductions shown in the fourth line of this table.

and 6% and are not uniform for the *e-e*, *e-t*, and *t-t* types of interactions.

(b) Comparing the two cluster $^6A_1$ calculations at $R=2.43$ Å shows that including V(ext) only slightly lessens the degree of reduction to a more uniform 3% to 4.5%.

(c) At all distances considered, the hypothetical $\bar{H}$ state, which is almost entirely composed of the excited quartet states, exhibits roughly 60% more orbital reduction than the pure $^6A_1$ ground state.

(d) The percentages of reduction decrease by roughly 60% as R(Mn-S) increases from 2.27 to 2.59 Å.

These observations can be understood semiquantitatively in the context of the discussion surrounding Eq. (1.1), from which

$$\bar{I}(ee)\simeq N_e^4\bar{I}_0(ee)\ , \tag{3.1}$$

$$\bar{I}(tt)\simeq N_t^4\bar{I}_0(tt)\ , \tag{3.2}$$

$$\bar{I}(et)\simeq N_e^4\bar{I}_0(et)\ . \tag{3.3}$$

$\bar{I}=\bar{J}$ or $\bar{K}$ from a particular cluster SCF and $\bar{I}_0$ is the corresponding free-ion value. N_e^2 and N_t^2 are identified as fractions of free-ion 3*d* *e* and 3*d* *t* AO character in the *e* and *t* MO's, respectively. Various sets of values are shown in the lower part of Table IV, using tabulated values of orbital reductions and Eqs. (3.1) and (3.2).

This analysis indicates a slightly smaller ($\leq 1\%$) amount of delocalization in the purely π-bonding *e* MO. In all cases, the *e* and *t* MO's are at least 96% atomic 3*d* in character, with only small increases ($\sim 1\%$) as R(Mn-S) increases in the range shown.

Virtually identical values of N_e^2 and N_t^2 are obtained from $\bar{I}=\bar{J}$ and from $\bar{I}=\bar{K}$. These values also show that Eq. (3.3) is nearly consistent with Eqs. (3.1) and (3.2) for average Coulomb interactions ($I=\bar{J}$) but it underestimates the reduction in the *e-t* average exchange integral ($\bar{I}=\bar{K}$) by as much as 22%. [The error in the estimated $\bar{K}(et)$ is ~ 0.0076 eV or ~ 60 cm^{-1} too small.]

2. *Orbital energies, ionization potentials, and electron affinities*

The 3*d*-like *e* and *t* MO's of the MnS_4 cluster are open-shell orbitals; both are spatially and energetically well separated from all closed-shell sulfur-type MO's. At the observed Mn-S distance in the ground state $^6A_1$ and including V(ext), the *e* and *t* orbital energies, $\varepsilon^0(e)$ and $\varepsilon^0(t)$, respectively, are ~ -0.59 a.u. The various S(3*p*)-like MO's have energies around -0.44 a.u. (i.e., ~ 4 eV higher) with a width of ~ 1.6 eV. All these MO's are much higher than the S(3*s*)-like MO's near -0.92 a.u. (see Table V).

All orbital energies drop by ~ 1 a.u., when V(ext) is included. In particular, the *e* and *t* MO's are lowered by 1.0867 and 1.0848 a.u., respectively, compared to the values of V(ext)=1.0672 and 1.1186 a.u. at the Mn and S sites in the crystal.

These valence-shell orbital energies vary almost linearly with R(Mn-S) over the range considered, at rates shown in Table V. The "band" of S(2*p*)-like MO's has extrema that are almost independent of R, although its internal structure does change. $\varepsilon^0(e)$ and $\varepsilon^0(t)$ rise to ~ 2 eV below the bottom of the S(2*p*) "band" when R(Mn-S) decreases to 2.27 Å.

The degree to which the *fixed* SCF MO's of $MnS_4^{6-}(^6A_1)$ may be used to estimate its vertical ionization potentials (IP) and electron affinities (EA), (i.e in the approximation underlying Koopmans's theorem[43] was examined by performing SCF calculations on MnS_4^{5-} and MnS_4^{7-} clusters, using the same Gaussian basis and V(ext). The states considered result from adding or removing one electron from the *e* or t_2 MO of MnS_4^{6-}, or from ionizing one nonbonding electron from the S(3*p*)-type $2t_1$ MO. Results are shown in Table VI, with computational specifics given in its footnotes.

All values of $\Delta E_{\rm SCF}$ are, of course smaller [by an amount termed the internal electronic relaxation energy (IERE)], because of reoptimization of cluster MO's in the final states. Removing the nonbonding S(3*p*) electron from $2t_1$ (which is distributed over the four ligands) produces an almost negligible net IERE; Koopmans's theorem appears accurate for such ligand-type MO's. (If symmetry constraints are relaxed, however, it is possible for the hole to localize toward just one ligand, thus increasing the internal relaxation energy.[44]) On the other hand, IERE substantially reduces the fixed-orbital estimates of IP and EA, when the number of highly localized 3*d*-type electrons changes. While each particular IP or EA varies by several eV over the range of distance, the corresponding IERE's are quite constant.

External electronic relaxation (bulk polarization) is difficult to assess accurately. The classical direct-reaction-field method,[45] using a lattice of 420 nearest sulfide ions and a dielectric constant of 5.2,[46] gives a crystal polarization effect of 4.6 eV for the addition or removal of one electron from the Mn site. SCF calculations on just the $(S_4)^{8-}$ group of the cluster at that site showed

TABLE V. Variation of orbital energies with Mn-S distance. From SCF on the $^6A_1$ state of MnS_4^{6-} with V(ext) included.

MO	ε (eV)[a]	$d\varepsilon/dR$ (eV/Å)
	3*d* type	
$e=3e$	−16.24	−8.36
$t=10t_2$	−15.78	−5.66
	S(3*s*) type	
$7a_1$	−25.03	−2.8
$7t_2$	−24.73	−3.3
	S(3*p*) type	
$8a_1$	−12.60	−0.6
$2e$	−12.35	−3.9
$2t_1$	−11.73	−5.1
$8t_2$	−12.44	−3.8
$9t_2$	−11.18	−1.3

[a]Open-shell orbital energies are given for *e* and *t*, and closed-shell values for the others. R(Mn-S)=2.43 Å.

that the intracluster contribution is 0.4 eV. Hence, the net polarization external to the cluster is estimated to be 4.2 eV. It is assumed constant for all ionization potentials (IP's) and electron affinities (EA's) of the clusters. Resulting estimates of IP's and EA's are entries labeled (i) in Table VI.

The estimated "$3dt$" IP lies at 6.6 eV, just above the top of the S($3p$) "band" and the "$3de$" IP lies 0.7 eV lower and just at the IP of $2t_1$, which is 1 eV above the bottom of the "band", all at $R=2.43$ Å. This picture is quite different from what would be predicted from SCF orbital energies and Koopmans's theorem.

From analysis of ultraviolet photoemission spectroscopy (UPS) and x-ray photoemission spectroscopy (XPS) measurements on the Cd-Mn-Te system, Webb *et al.*[47] concluded that the Mn d^5 level lies 3.5 eV below the top of its valence band. Then, assuming literature values of work functions and a constant ionization energy for the Mn d^5 level of 9.7 eV, they position the Mn d^5 ionization in ZnS at 9.7 eV below vacuum, i.e., 2.4 eV below the top of the valence band, which is 7.3 eV below vacuum[48] and is about 6-eV wide. From independent XPS measurements, Langer, Hehner, and Weichert located the Mn $3d^5$ level at 2.2 eV below the top of the valence band.[49] Orlowski, Kopalko, and Chab[50] studied the closely related Cd-Mn-Se system. They noted the typical $3d^5$ peak (in this case also 3.5 eV below the top of the valence band) and commented on additional structure in the valence band at ~ 0.9 eV above the $3d^5$ peak, which they ascribed to p-d hybridization of band and Mn states.

First, it should be noted that the effect of the hole localization in S($3p$) ionized states is to reduce the "S($3p$)" IP with respect to the "$3d$" IP's. In CuCl and NiO this effect is about 3 eV. A similar effect in MnS_4 would position the onset of Mn states considerably below the top of the valence band. Second, the absolute values of the calculated IP's would increase significantly (of the order of 2 eV) if the loss of atomic (i.e., dynamical) correlation ener-

TABLE VI. Calculated vertical ionization potentials V_{IP}, electron affinities ε_{EA}, and internal electronic relaxation energies (IERE) for MnS_4^{6-} (values in eV).

$MnS_4^{6-}(e^2t^3\text{-}^6A_1)$ to	Footnote	R(Mn-S) (Å) 2.27	2.43	2.59
$MnS_4^{7-}(e^3t^3\text{-}^5E)$	a,b	9.41	8.30	7.11
	c	6.08	5.05	3.91
	d	3.33	3.25	3.20
	e		0.9	
$MnS_4^{7-}(e^2t^4\text{-}^5T_2)$	a,f	10.38	9.25	8.03
	c	6.34	5.25	4.06
	d	4.04	4.00	3.97
	e		1.1	
$MnS_4^{5-}(e^2t^2\text{-}^5T_2)$	a,g	14.26	15.79	17.25
	c	9.22	10.83	12.30
	d	5.04	4.96	4.95
	e		6.6	
$MnS_4^{5-}(e^1t^3\text{-}^5E)$	a,h	14.93	16.25	17.58
	c	10.08	11.54	12.91
	d	4.85	4.71	4.67
	e		7.3	
$MnS_4^{5-}(2t_1^{-1}e^2t^3\text{-}^7T_1)$	a,i		11.72	
	c		11.49	
	d		0.23	
	e		7.3	

[a]Calculated from frozen MO's of $MnS_4^{6-}(^6A_1)$; see Ref. 37 for general procedures. Appropriate open-shell formulas are given in footnotes (b) to (i), as indicated.
[b]$\varepsilon_{EA}=\varepsilon^0(e)+2\bar{K}(ee)$.
[c]ΔE_{SCF}.
[d]Internal electronic relaxation energy, IERE = (a)−(c).
[e]$\Delta E_{SCF}-4.2$ eV, the estimated polarization of the external surroundings of the cluster. (See text. The same value for external electronic relaxation is assumed for ligand ionizations.)
[f]$\varepsilon_{EA}=\varepsilon^0(t)+3\bar{K}(tt)$.
[g]$V_{IP}=-\varepsilon^0(t)$.
[h]$V_{IP}=-\varepsilon^0(e)$.
[i]$V_{IP}=-\varepsilon(2t_1)$.

gy were taken into account. Hence, it seems that considering the experimental and theoretical assumptions made, the estimated IP's agree remarkably well with these data. Our results suggest that ionization from the t-type $3d$ MO (estimated at 6.6 eV, not including loss of atomic correlation) is what adds structure to the upper band and that the e-type $3d$ MO ionization (estimated at 7.3 eV) corresponds to the more-isolated, so-called $3d^5$ peak.

Despite discrepancies of 2–3 eV, these cluster-based calculations provide a prediction of ionization processes fully consistent with the structure added by Mn^{2+} to the UPS and XPS spectra of the II-VI host and clearly demonstrate the major significance of electronic relaxation corrections required.

According to results in Table VI, total energies of both MnS_4^{7-} (Mn^+) and MnS_4^{5-} (Mn^{3+}) are higher than the MnS_4^{6-} (Mn^{2+}) ground state, but they vary oppositely with R(Mn-S). This suggests examining electron transfer (Mn^{2+} disproportionation) between two clusters in the crystal:

$$Mn^{2+}(R_0)+Mn^{2+}(R_0)\rightarrow Mn^{+}(R_0+\delta_1) + Mn^{3+}(R_0+\delta_3)\ ,$$

where $R_0=2.43$ Å. Four quintet-quintet pair states result, with $Mn^+(^5E)+Mn^{3+}(^5T_2)$ being the lowest. With $\delta_1=\delta_3=0$ and using frozen Mn^{2+} MO's (Koopmans's theorem),

$$\Delta E=\varepsilon^0(e)-\varepsilon^0(t)+2\bar{K}(ee)=\varepsilon_{EA}+V_{IP} =8.3+15.8=24.1\ \text{eV}\ .$$

Internal and external electronic relaxations reduce ΔE to $0.9+6.6=7.5$ eV (Table VI). If the two sites are nearest neighbors, the hole-particle interaction further reduces ΔE by $e^2/r=-3.6$ eV [$r=3.96$ Å, for R(MnS)$=2.43$ Å], to 3.9 eV. This estimate may be too small, for the same reasons as with the IP's just discussed, although it is remarkably close to McClure's estimate of 4 eV.[51]

Following electron transfer, the S ligands at the Mn^+ and Mn^{3+} sites also may relax along the totally symmetric modes, at least. Now with $\Delta E=\Delta E(\delta_1,\delta_3)$, and derivatives evaluated from data in Table IV,

$$\Delta E(\delta_1,\delta_3)\simeq\Delta E(0,0)+(\partial\varepsilon_{EA}/\partial\delta_1)\delta_1+(\partial V_{IP}/\partial\delta_3)\delta_3 \simeq 3.9-6.8\delta_1+9.6\delta_3$$

in eV and Å. [Remember that $\Delta E(\delta_1,\delta_3)$ is the vertical energy of the two-site CT state above the ground state, also at (δ_1,δ_3).] The calculated values of the derivatives indicate that the *relaxed* equilibrium values of δ_1 and δ_3 should be roughly in the ratio $\delta_1/\delta_3=-6.8/9.6=-0.7$. Then, for example, if $\delta_3=0.05$ Å, ΔE would decrease by 0.7 eV. Further stabilization from Jahn-Teller distortions at the Mn^+ and Mn^{3+} sites must also be considered.

3. *Variation of ground-state total energy with distance*

No attempt was made to study the adiabatic potential-energy surface (APES) of the ground state in detail. A few suggestive features will be noted, however, from Table VII which gives relative values of total energy for MnS_4^{6-} and for a point-charge model of the cluster.

The free cluster is calculated to be roughly 6 eV more stable than the separated ions. (RCT-CI, considered below, lowers the ground state by an additional 0.3 eV.) V(ext) makes a small difference at the 2.59 Å distance, but in either case the theoretical minimum lies below the crystal distance, 2.43 Å. Subtracting the classical point charge, $(+2)(-2)_4$, contribution to the binding energy indicates that the total of all types of repulsion energies within the cluster increases very rapidly at shorter distances, roughly as R^{-14}.

Clearly, repulsive contributions must be added to V(ext) in order to obtain realistic equilibrium distances and force constants for all states of the cluster. Such potential functions have been formulated (see Refs. 1 and 52, for example). Pueyo and co-workers[53] have applied theirs to a number of transition-metal ions in fluoride compounds with remarkably good success. It would likely improve the APES's in this system also. On the other hand, we assume that its omission from V(ext) should have no greater effect on vertical excitations within the cluster than omission of V(ext) itself.

C. *d-d* excitation energies

1. *Pure configurational excitation energies*

The importance of V(ext) and IERE upon calculated d-d excitation energies will be considered first. These are examined by determining their effects upon energies of the pure configuration-state functions (CSF's), $|is\Gamma\rangle$. Independent SCF calculations were performed upon most CSF's, with and without V(ext). Excitation energies were also calculated in the frozen-orbital approximation, using MO's from both $^6A_1$ and the average-of-configurations states $\bar{H}$. Results are shown in Table VIII.

V(ext) has a very small effect on values of ΔE_{SCF}; all shifts calculated are <0.04 eV $\simeq 300$ cm^{-1}. Within the cluster model this suggests that any larger differences in the d-d spectra observed for Mn^{2+} in ZnS, CdS, and HgS are due to differences in geometry at the Mn^{2+} site.

Similar to the cases of IP's and EA's, frozen-orbital ΔE's calculated from MO's of the $^6A_1$ ground state are all larger than the corresponding ΔE_{SCF}'s; these IERE's (ΔE_{relax}) range from -0.07 to -0.24 eV, roughly in proportion to ΔE. Values of ΔE_{relax} obtained from the $\bar{H}$ SCF, however, average one-third the magnitude. Some are positive, since the SCF calculation on the $\bar{H}$ state, heavily weighted with the quartet states, gives a much better representation of their energies. Compared to frozen-orbital total energies from the $^6A_1$ SCF, the quartets from $\bar{H}$ average about 0.07 eV lower while the ground state is 0.07 eV higher than its independent SCF value. Clearly the $\bar{H}$ SCF furnishes the better choice of basis for frozen orbital calculations of excitation energies.

Since similar observations apply to the other two distances, further calculations reported in the next section will be based upon the $\bar{H}$ SCF results including V(ext).

One can anticipate, in the context of the CF model, the weak-field character of the cluster states from the order

TABLE VII. Variation of SCF total energy with Mn-S distance, relative to $R = 2.43$ Å (in eV).

R (Å)	With V(ext) MnS_4^{6-}	MnS_4^{6-}	Without V(ext) $(+2)(-2)_4$ model[c]	Repulsion[d]
∞		+5.81	+5.81	0
2.59	−1.94	−2.31	−1.44	+0.87
2.43	0[a]	0[b]	−1.92	+1.92
2.27	+3.58	+3.51	−2.46	+5.97

[a]SCF total energy is −2744.219 88 a.u.
[b]SCF total energy is −2737.467 74 a.u.
[c]Electrostatic potential energy relative to MnS_4^{6-} at $R \to \infty$.
[d]Internal repulsion energy, difference between previous two columns.

of the (strong field limit) energies of the $^4T_1$ and $^4T_2$ CSF's, given in Table VIII. Energies of $^4T_1$ CSF's increase in the order e^3t^2, e^1t^4, e^2t^3, whereas the $^4T_2$ order is e^2t^3, e^3t^2, e^1t^4. One expects the t MO's to lie above the e MO's by $\Delta = \frac{40}{9}Dq$, producing the strong-field order e^3t^2, e^2t^3, e^1t^4 in both cases. The orders found can be analyzed by equating differences in values of ΔE_{SCF} calculated with V(ext) to the simple CF model results.[31] One obtains (in eV)

$$E(e^2t^3\,{}^4T_2) - E(e^3t^2\,{}^4T_1) = 0.212 = 3B - C + \Delta ,$$

$$E(e^3t^2\,{}^4T_2) - E(e^1t^4\,{}^4T_1) = 0.283 = 8B - 2\Delta ,$$

$$E(e^1t^4\,{}^4T_2) - E(e^2t^3\,{}^4T_1) = -0.316 = -B - C + \Delta .$$

Solving these equations gives $B = 1065$ cm^{-1}, $C = 4602$ cm^{-1}, and $Dq = 700$ cm^{-1}; the Racah parameters are larger than the semiempirical values quoted in Table II but close to the values calculated from the SCF on the ^6S state. Since this effective Dq is much smaller than the differential effects on d-d interaction energies, the weak-field behavior should dominate.

This conclusion again stresses the inadequacy of single-configuration MO results (based upon the strong-field limit)[20,21,54–56] and reemphasizes that LF-CI at least plus CEC, which is formally equivalent to the intermediate-CF scheme, is necessary.

2. *Quartet states and excitation energies, including LF-CI and CEC*

Using the procedure described in Sec. II C 1, and SCF results for the $\bar{H}$ state including V(ext), excitation energies were calculated for each of the three distances. See Table IX. For $R = 2.43$ Å the consequences of successively including LF-CI and CEC and then omitting V(ext) are shown. The seven lowest excitation energies are graphed as a function of R(Mn-S) in Fig. 2 in a manner that parallels the CF diagram, Fig. 1.

The compositions of the LF-CI functions are indicated in Table X according to percentages of the individual CSF's [$= 100C^2_{n,i\Sigma\Gamma}$, from Eq. (2.4)] and, approximately, of the free-ion states contributing. The latter values are obtained after transformation of Eq. (2.4) with the *free-*

TABLE VIII. Energies of configurational state functions relative to $^6A_1$; effect of V(ext) and relaxation energies at $R = 2.43$ Å. (Energies in eV.)

Promotion $^6A_1(e^2t^3)$ to	without V(ext)	ΔE_{SCF} with V(ext)	Foot-note	Effect of V(ext)	ΔE [with V(ext)] from $^6A_1$	from $\bar{H}$	ΔE_{relax} [with V(ext)] from $^6A_1$	from $\bar{H}$
$^4T_1(e^1t^4)$		4.604	a		4.688	4.573	−0.084	+0.031
$^4T_1(e^2t^3)$	5.811	5.837	b	+0.026	6.065	5.875	−0.228	−0.038
	5.861	5.883	a	+0.022	6.605	5.875	−0.181	+0.008
$^4T_1(e^3t^2)$	3.978	3.943	a	−0.035	4.052	3.914	−0.108	+0.029
$^4T_2(e^1t^4)$		5.567	a		5.763	5.617	−0.196	−0.050
$^4T_2(e^2t^3)$	4.134	4.141	b	+0.007	4.239	4.103	−0.098	+0.038
	4.146	4.155	a	+0.009	4.239	4.103	−0.083	+0.052
$^4T_2(e^3t^2)$	4.919	4.887	a	−0.032	5.126	4.958	−0.240	−0.071
$^4A_1(e^2t^3)$	3.802	3.809	a	+0.007	3.857	3.744	−0.043	+0.065
$^4E(e^2t^3)$								
$(^2E * {}^3A_2)$		4.209			4.282	4.156	−0.072	+0.053
$(^4A_2 * {}^1E)$		4.329			4.416	4.298	−0.088	+0.031
$^4A_2(e^2t^3)$					6.520	6.349		

[a]SCF calculations using energy expressions forcing degenerate wave functions to be spatially equivalent.
[b]SCF calculations using energy expressions derived directly from the wave function, allowing for spatial differences to occur within degenerate sets of MO's.

TABLE IX. Excitation energies for MnS_4^{6-} (in eV). From $\overline{H}$ SCF including LF-CI and CEC.

	With V(ext), $R=2.43$ Å			No V(ext) $R=2.43$ Å		With V(ext) LF-CI+CEC	
$^6A_1$ to	Pure CSF[a]	LF-CI only	LF-CI +CEC	LF-CI +CEC	Max. in spect.[b]	$R=2.27$ Å	$R=2.59$ Å
$a\,^4T_1$	3.914	3.626	2.843	2.872	2.34	2.664	2.960
$a\,^4T_2$	4.103	3.707	2.992	2.988	2.49	2.882	3.058
$^4A_1$	3.774	3.744	3.035	3.023		2.959	3.084
					2.67		
$a\,^4E$	4.156	3.765	3.056	3.039		2.990	3.097
$b\,^4T_1$	4.573	4.449	3.478	3.421	2.89	3.490	3.465
$b\,^4T_2$	4.958	4.616	3.590	3.587	~3.17	3.452	3.675
$b\,^4E$	4.298	4.688	3.672	3.652		3.590	3.724
$c\,^4T_1$	5.875	6.287	4.914	4.886		4.789	4.994
$^4A_2$	6.349	6.349	4.972	4.947		4.874	5.037
$c\,^4T_2$	5.617	6.354	4.994	4.952		4.926	5.042

[a]From Table VIII.
[b]From Table I; final assignments of the fourth and fifth bands are not made at this level of calculation, however.

ion coefficients $\langle iS\Gamma|SL\rangle_0$ defined in Eq. (2.9).

With the qualitative inverse dependence of Dq upon R in mind, the present calculated excitation energies show a considerable similarity to the CF diagram in its low-Dq region between 250 and 500 cm^{-1}. The intervals between $a\,^4T_1$ and $b\,^4E$ are both ~7000 cm^{-1}, as is the experimental separation between the first and fifth bands, and $b\,^4T_1$ lies below $b\,^4T_2$.

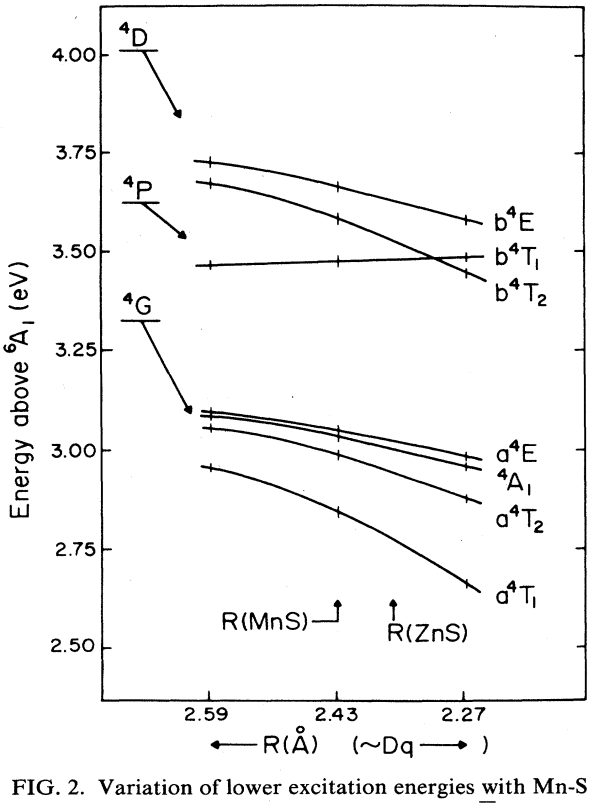

FIG. 2. Variation of lower excitation energies with Mn-S distance. Frozen-orbital calculations from SCF on $\overline{H}$ state, including LF-CI, CEC, and V(ext). R(MnS) and R(ZnS) are the metal-S bond distances in the respective phases.

Energies of the calculated intraconfigurational transition to $^4A_1$ and $a\,^4E$ show the expected dependence upon distance[14] due to changes in orbital reduction of d-d electrostatic interactions [$\overline{K}(et)$ in particular], as shown in Table IV. In contrast to semiempirical predictions,[12] the present frozen-orbital calculations show the reverse ordering of $^4A_1$ and $a\,^4E$, with a separation of 170 cm^{-1}. This result simply follows from the fact that the two excitation energies are determined by a delicate balance of four nonuniformly reduced d-d interaction integrals calculated from the SCF procedure. It is independent of CEC, since $^4A_1$ and $a\,^4E$ are both derived only from ^4G (Table X). The slight differences between relaxation energies (Table VIII) may reduce this separation somewhat, but are unlikely to reverse the order. The SCF plus LF-CI and CEC calculation, which fully quantifies the semiempirical CF schemes, therefore produces the reversed ordering. (RCT-CI, discussed below, modifies this conclusion, however.)

As $R\to\infty$, the cluster ΔE's should approach the free-ion ΔE's as limits. Except for $a\,^4T_1$ and $a\,^4T_2$, all states at $R=2.59$ Å are already nearly free-ion in character (Table X) and extrapolate monotonically; the gaps shown in Fig. 2 reflect orbital reductions of d-d interaction integrals and to a lesser extent the small difference between orbital energies $\varepsilon^0(t)$ and $\varepsilon^0(e)$ (Table IV) remaining at 2.59 Å. On the other hand, even at 2.59 Å, $a\,^4T_1$ and $b\,^4T_1$ show considerable mixing of ^4G and ^4P character (Table X), or equivalently high pure-CSF characters (88.7% e^3t^2 and 78.7% e^1t^4, respectively) that indicate a stronger dependence upon $\varepsilon^0(e)-\varepsilon^0(t)$. Combined with orbital reductions, these effects place $a\,^4T_1$ and $b\,^4T_1$ relatively low compared to ^4G and ^4P, respectively. Indeed, at this level of CI, $b\,^4T_1$ may pass through a minimum beyond $R=2.59$ Å, quite unlike the simple CF diagram, and surely does after RCT-CI effects are included (below).

TABLE X. Composition of states of MnS_4^{6-} (in percent) at $R=2.43$ Å and 2.59 Å. (Values in parentheses are for $R=2.59$ Å.) From $\bar{H}$ SCF including LF-CI, CEC, and V(ext).

	MO CSF's			Approximate free-ion states			
	e^1t^4	e^2t^3	e^3t^2	^4G	^4P	^4D	^4F
$^6A_1$		100		100			
$a\,^4T_1$	5	4	91	69	31		0
	(8)	(3)	(89)	(75)	(25)		
$a\,^4T_2$	15	55	30	99		0	1
	(16)	(56)	(27)	(99)		(0)	(1)
$^4A_1$		100		100			
$a\,^4E$		100		99.9		0.1	
$b\,^4T_1$	80	18	2	30	69		0
	(79)	(18)	(3)	(25)	(75)		(0)
$b\,^4T_2$	15	45	40	0		97	3
	(18)	(44)	(38)	(0)		(98)	(2)
$b\,^4E$		100		0.1		99.9	
$c\,^4T_1$	15	78	7	1	0		99
	(13)	(79)	(8)	(0)	(0)		(100)
$^4A_2$		100					100
$c\,^4T_2$	69	0	31	1		3	96
	(66)	(0)	(34)	(1)		(2)	(98)

3. *Excitation energies, including RCT-CI and CEC*

Following the procedures described in Sec. II C 2, RCT-CI calculations were performed for the T_d geometry at $R=2.43$ Å. In order to account for relaxation effects (IERE), CI calculations for the ground state were carried out with $^6A_1$ SCF orbitals, and for the d^5 quartets with $\bar{H}$ SCF orbitals.

Detailed study of the CT states themselves is beyond the scope of the present study. A prior qualitative description of them and how they interact with the d^5 quartets, however, aids in analyzing the results obtained.

In the frozen-orbital approach the lowest CT states belong to the $d^6(2t_1)^{-1}$ configuration followed by states with the ligand hole in the $9t_2$, $2e$, $8t_2$, and $8a_1$ orbitals, respectively. An SCF calculation on the average of the $^7T_1$ and $^7T_2$ states of the $e^3t_2^3(t_1)^{-1}$ configuration has shown that the lowest SCF CT excitation energy is 11.5 eV. This is not a reasonable estimate of the "true" CT excitation energy, since localization effects on the ligands (which may be ~ 3 eV) are neglected. From this SCF result it can be concluded that CT excitation energies are rather larger in MnS_4^{6-} than in $CuCl_4^{2-}$ or $CuBr_4^{2-}$ but similar to those in NiO_6^{9-}, the three systems studied recently using very similar methods.[29,30] RCT-CI effects comparable to those in the NiO_6 system should thus be found in MnS_4^{6-}. Because of the much greater number of d^n states, however, there is a much greater variety of RCT-CI effects possible in the Mn^{2+} system.

The CT CSF's that contribute to the sextet ground state belong to the $e^3t_2^3(2e)^{-1}$ configuration (a single π electron replacement) and to the $e^2t_2^4(8t_2)^{-1}$ and $e^2t_2^4(9t_2)^{-1}$ configurations (σ replacement). The major contribution to the quartets come from the states depicted in Fig. 3. If the energies of d^6 states (which are coupled to the holes in the sulfur-type valence MO's) are estimated to be in the order

$$e^4t_2^2 < e^3t_2^3 < e^2t_2^4 < e^1t_2^5 ,$$

the scheme given in Fig. 3 is obtained. From this scheme some predictions can be made of the contribution of CT CSF's to the d^5 states. First, it is seen that the second group of d^5 states (^4P,^4D derived states) will be more affected than the first group (^4G states). Secondly, in each group of states the effect will be largest for the d^5 state containing the largest e^3t^2 CSF contribution, since the CT CSF's perturbing such states have the lowest energy.

This means, in particular, that we must expect a larger effect upon $b\,^4T_2$ than upon $b\,^4T_1$ or $b\,^4E$ in the second group of states. Of them $^4T_2$ is closest to its perturbing CT states; furthermore, $b\,^4T_2$ is 40% e^3t^2 in character, compared to 2% and 0% for $b\,^4T_1$ and $b\,^4E$, respectively (Table X). The third group of d^5 states is not depicted in Fig. 3 but large effects upon them are also expected.

On the basis of these considerations, the RCT-CI results, displayed in Table XI and Fig. 4, can now be analyzed.

The effects of RCT-CI relative to the LF-CI excitation energies are not uniform. The most important feature is that all quartets are depressed more than the sextet and the discrepancy in the $^6A_1$-$a\,^4T_1$ gap is reduced by half, to 0.34 eV. Within the first group of states the $a\,^4T_1$-$a\,^4T_2$ separation remains the same, but the $^4A_1$ and $a\,^4E$ states have a relatively higher energy. The $^4A_1$-$a\,^4E$ degeneracy is almost restored.

The anticipated differential effects within the second group of states is so large that $b\,^4T_2$ passes below $b\,^4T_1$, a result amplified by the inclusion of CEC.

The highest group of d-d excitations shows the largest

decrease in energy, but this is insufficient to bring it close to the second group. The only other Mn^{2+} state that might occur near the second group is $^2T_2(^2I)$. At the LF-CI+CEC level, this state is 0.5 eV above $b\,^4E$. No RCT-CI calculations were done upon doublet states. To make this $^2T_2$ state come close to $b\,^4E$, however, would require a reduction of about 1 eV through RCT-CI. Such a reduction is large, but not impossible.

The first six transitions in the RCT-CI+CEC spectrum span 0.85 eV, just like in the LF-CI+CEC spectrum and in the experimental spectrum. The overall agreement between experimental and theoretical spectra is much better at the RCT-CI level than at the LF-CI level. First of all, the $^6A_1$-$a\,^4T_1$ splitting is much smaller in

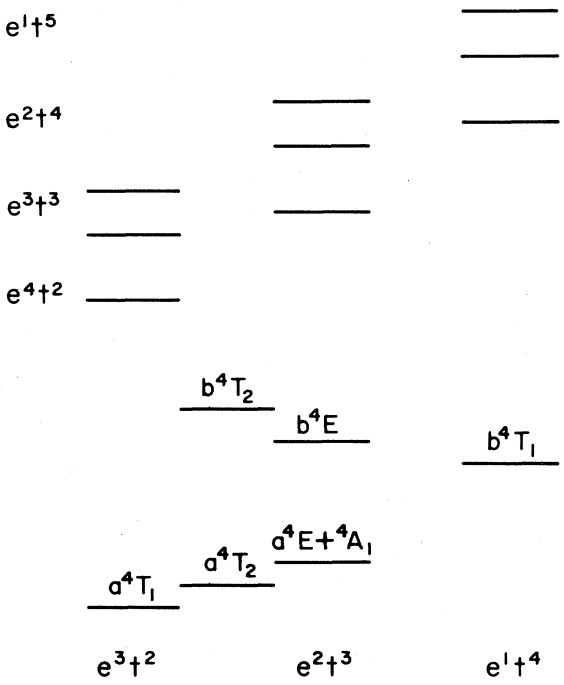

FIG. 3. Schematic representation of relative energies of the quartet d^5 levels and their respective perturbing excited CT levels. The vertical elevation and horizontal position of each d^5 level (denoted by a term symbol) are determined by its principle $e^m t^n$ character (shown in Table X); the $^4T_2$ levels show a large mixing of e^2t^3 and e^3t^2 and are therefore drawn between the corresponding columns. The subgroups of CT states (upper half of figure) are horizontally separated according to the $e^m t^n$ configuration from which they are derived. The estimated relative positions of the d^6 CSF energies are indicated by symbols in the upper left side. They largely determined the elevations of the CT CSF's. The ordering within subgroups of CT levels in each column is qualitative. The lowest line in each subgroup corresponds to $e^{m+1}t^n(2e)^{-1}$ states; the upper two lines correspond to $e^m t^{n+1}(8t_2)^{-1}$ and $e^m t^{n+1}(9t_2)^{-1}$ states. In first order, each d^5 state is perturbed only by CT states of the same symmetry in the same column or, for $^4T_2$ states, the two adjacent columns in proportion to their e^3t^2 and e^2t^3 compositions.

the RCT-CI calculations. Secondly, the separation between $a\,^4T_2$ and $^4A_1+a\,^4E$, which is too small in the LF-CI spectrum, is somewhat larger in the RCT-CI spectrum. The $a\,^4T_1$-$a\,^4T_2$ splitting comes out equally well in both calculations.

Several of the changes in the RCT-CI+CEC spectrum compared to the LF-CI+CEC spectrum point in the direction of a larger effective Dq value, especially the reversed order of the $b\,^4T_1$ and $b\,^4T_2$ states. However, a larger value of Dq alone cannot explain the larger energy gain of the several groups of levels, i.e., the third group has a larger energy gain than the first one. It is clear that the higher levels are stabilized most by the CT states, but throughout the whole spectrum there is a differentiating effect that stabilizes e^3t^2 states more than e^1t^4 states.

These relative RCT-CI effects are roughly measured by the percent CT CSF character of the RCT-CI wave functions obtained; see Table XI. The smallest CT contribution (2%) is to the sextet ground state and 2% more than that to the first and second groups of excited states, *except* $b\,^4T_2$, whose additional 4% CT contribution agrees with its much greater depression.

The calculated spectrum is still not quite in agreement with the experimental one, i.e., the $^6A_1$-$a\,^4T_1$ splitting is still somewhat too large and the separation between the third and fourth bands is too large. This is not due to relaxation effects; they only contribute about 0.1 eV in the LF-CI spectrum (Sec. III C 1) and are largely incorporated by the RCT-CI. On the one hand it seems that the agreement would improve if the RCT-CI effects were just slightly larger. Since the RCT-CI carried out here has only a limited number of virtuals, inclusion of more might enlarge the effects, as might extension of the valence set and extension of RCT-CT to FOCI. On the other hand, the MnS_4^{6-} CT CSF states used in the RCT-CI calculation probably lie too high, as previously noted. If, in fact, they occur lower in energy by several eV, they would depress the quartets relative to $^6A_1$ by an even greater extent, further improving agreement with experiment.

As pointed out earlier, some authors[12,57] have tried to show that $a\,^4E$ always lies below $^4A_1$ and in some parametrization schemes this is true. However, in the LF-CI calculations performed in this work the differences between these states are so small that they cannot be accounted for in the parametrization schemes. Since both RCT-CI and orbital relaxation further change the ordering, it does not seem particularly useful to discuss the order of these states in great detail, particularly without including spin-orbit effects as well.

CI with states having an electron transferred from Mn to the conduction band of the host might be considered also to play a role. Since E_{gap} is nearly constant over the range of x, unlike its behavior in $Zn_{1-x}Mn_xSe$, the degree of interaction between conduction-band and d states should be constant. Indeed, the Mn d spectrum in ZnS appears almost independent of x, while a slight variation is found in the Se system (Table I). In either case, however, such interaction must be small.

RCT-CI calculations with more CT CSF's and at other

TABLE XI. Evolution of excitation energies for MnS_4^{6-} (in eV) at $R = 2.43$ Å, based upon the relaxed–charge-transfer-state (RCT-CI) wave functions and including V(ext).

State	LF-CI+CEC[a]	RCT-CI	RCT-CI+CEC	Max. in spect.[c]	Percent CT CSF of state[d]
$^6A_1$	0.00	(−2744.2304)[b]	0.0	0.0	2
$a\,^4T_1$	2.84	3.46	2.68	2.34	4
$a\,^4T_2$	2.99	3.55	2.83	2.49	4
$^4A_1$	3.04	3.67	2.96	2.67	3
$a\,^4E$	3.06	3.67	2.96	2.67	3
$b\,^4T_2$	3.59	4.33	3.31	2.89	6
$b\,^4T_1$	3.48	4.36	3.39	3.19	4
$b\,^4E$	3.67	4.54	3.52		4
$c\,^4T_1$	4.91	5.74	4.36		13
$c\,^4T_2$	4.99	5.94	4.58		8
$^4A_2$	4.97	6.04	4.66		5

[a]From Table IX.
[b]Total energy (in a.u.) calculated with $^6A_1$-optimized orbitals. The excited states were calculated with H-optimized orbitals.
[c]See Table I.
[d]Percent of CT-CI wave function that arises from CT CSF's.

values of R(Mn-S) may cast some light on this problem. While the absolute energies of the T_d d^5 states rise moderately on either side of their minima near 2.43 Å, the corresponding energies of the RCT-CI states should drop monotonically with R. The extent of RCT-CI interaction effects upon the d^5 states should therefore be proportional to R.

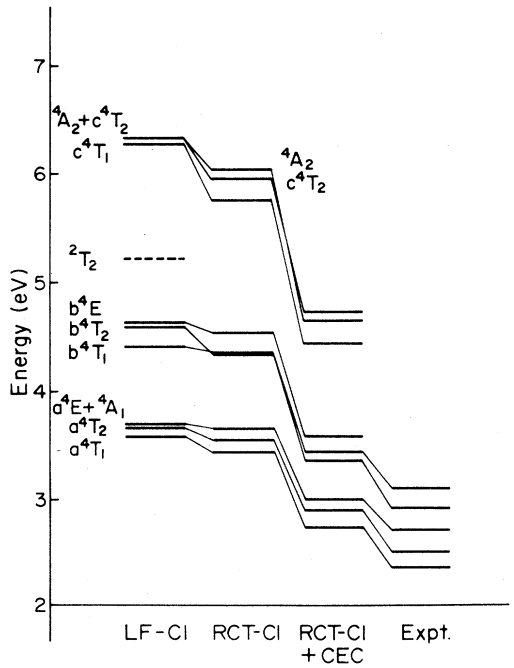

FIG. 4. Evolution of the d-d spectrum of $MnS_4^{6-}+V$(ext). Transition energies are given with respect to the $^6A_1$ ground state. Data from Tables I, IX, and XI.

IV. DISCUSSION

A. MO versus VB model of transition-metal deep centers

The MO model as used in cluster calculations and one-electron band theory (its solid-state equivalent) have been criticized as inadequate for characterizing electronic d states of deep centers, such as Ni^{2+} in NiO (Ref. 58) and Mn^{2+} in ZnS, as treated here. Instead, there has been suggested a formulation based upon valence-bond (VB) -type wave functions, which are linear combinations of local d^n states of the individual metal ion and CT states having one or two electrons transferred from symmetry-adapted ligand orbitals L to $3d$ AO's of the metal. That is, they are combinations of states from the configurations d^n, $d^{n+1}L^{-1}$, and $d^{n+2}L^{-2}$.[59] In *form*, these wave functions would result from an expansion of a single-configuration, many-electron wave function based upon MO's like those in Eq. (1.1). They have, consequently, more variational freedom, permitting greater contribution of the CT components to the higher-energy d^n states than to the ground d^n state and thus a reduction in the total width of the d^n states.

Just as in the elementary comparison of the VB (covalent plus ionic structures) and MO (bonding plus antibonding) descriptions of the H_2 molecule, the same additional variational freedom is added to the MO-based cluster model, by including appropriate CI with its CT states. Hence, the comparative virtues of the two approaches depend upon the elaborateness of the wave function required to achieve an acceptable level of agreement with experiment and upon the mechanisms required to produce the numbers.

The first-principles cluster-model MO-based results reported here and for the NiO and CuCl systems[19] document again the quantitative inadequacies of a single-configuration description and the major significance of

the particular electron-correlation effects encompassed by the LF-CI and CEC additions to the wave functions and excitation energies. Further, they suggest the magnitude of residual effects, perhaps chiefly from CT-CI contributions to correlations.

The molecular (RCT-CI) and atomic (CEC) correlation effects are not easily incorporated into an effective one-electron model like ligand-field theory. Like the long-known atomic correlation situation, the present work documents that metal-ligand covalency (or electron delocalization) effects are only partially determined in HF-MO calculations alone. A major contribution comes from RCT-CI, along with significant effects upon excitation energies. It is not clear whether RCT-CI effects can be described in an effective one-electron scheme.

The latter contributions clearly fall outside the assumptions of (weak-field–based) ligand-crystal-field theory and account for the difficulties encountered in those attempts to parametrize the experimental transition energies. There is no physical justification to represent *two*-particle electron-correlation effects introduced by CEC-type terms in the wave function by one-particle orbital reduction factors applied to free-ion Racah parameters combined with adjustments in the CF splitting parameter Dq.

Additional covalency introduced by the RCT-CI terms may perhaps be included in the effective orbital reduction parameter scheme; there is, however, no reason to believe that it could also encompass the CEC effect.

CT-CI effects clearly compromise the traditional semiempirical CF fitting procedure in such systems and complicate *ab initio* approaches as well.

B. Cluster model versus interactions with extended host

An alternative to the cluster model has been implemented within the framework of the impurity model for defect solids using the Hamiltonian introduced by Anderson.[60] Matrix elements, on the basis for the VB-type wave function, thereby become expressible as sums of a few physically well-defined characteristics of the system.[61] On the other hand, calculated results are extremely dependent upon numerical values assigned to those characteristics and it is nearly impossible to derive absolute magnitudes for the parameters on the basis of simple arguments.[62] This understandable feature also makes it difficult to obtain detailed quantitative comparisons to *ab initio* cluster-model results.

The relevance of certain other features in the application of the impurity model are noted.

(a) It should be formulated to include nonorthogonality among components of the VB-type wave function, i.e., that overlap integrals of the types $\langle d|L\rangle$ and $\langle L_i|L_j\rangle$ are generally nonzero. Although they are small in these "ionic" systems, it has been shown that they introduce major contributions to the splitting of energies of the d^n states that can be understood by chemical arguments.[20,21] Omitting this independent contribution to excitation energies from semiempirical treatments may force other parameters to assume unphysical values.

(b) Practical implementation of the impurity model involves summation over the band states of the host in the course of defining the spatial character of the L functions and their effective energies relative to the d^n levels. This procedure creates Wannier orbitals, localized about the impurity site, from the manifold(s) of band functions. One may regard the ligand orbital functions used in the cluster model to be one specific and well-defined approximation to Wannier function.[63] Orthogonality to other remaining Wannier functions is assumed. Furthermore, since a unitary transformation connects the Bloch and Wannier sets, this prescription provides an integral number of electrons to be assigned to the cluster.[63] Questions remain, however, about the nonlocal aspect of the exchange potential from the remaining electrons of the host.

(c) The transformation of band functions to Wannier functions and their separation into one set, localized at the impurity, and the set of all others, localized at all sites outside, may explain one of the questions remaining from this cluster treatment of MnS_4. Namely, what contribution to energies of the d states should be expected from CI with states involving charge transfer between the metal (impurity) site and (band) states of the host?

As noted in the Introduction, the observed positions of the Mn d bands in $A^{II}B^{VI}$:Mn^{2+} materials appear only slightly sensitive to Mn composition and, therefore, to the relative position of the band-to-band transition-energy gap E_g of the II-VI host. That is, as E_g rises above the ${}^6A_1 \rightarrow a\,{}^4T_1$ transition energy, for example, to ~ 0.5 eV higher, the d transition remains fixed within a few hundredths of an eV.

This observation may now be understood, most easily within the context of perturbation theory. The influence of the jth CT state upon the ith d^n state is measured by $(H'_{ij})^2/(E_i - E_j)$. Even though $(E_i - E_j)$ may vary by several eV, the influence will be small, if H'_{ij} is small. The integrals H'_{ij} involve the overlap distribution (product) of the d-type MO and the MO from which the electron is transferred. In the cluster CT states included in this work, both MO's are large within the cluster; their product and therefore the resulting value of H'_{ij} are relatively large. Both H'_{ij} and $E_i - E_j$ are fixed by the cluster calculation and the combined contribution is independent of composition.

On the other hand, if the jth CT states involves a function outside the cluster, the spatially separated d and CT MO functions overlap to a far smaller extent, decreasing exponentially with their separation. Their H'_{ij} is much smaller and most are near to zero. Except possibly from Wannier-type CT states involving the nearest-neighboring sites, CT-CI contributions from states external to the cluster should be very small, independent of $(E_i - E_j)$, i.e., of E_{gap}.

In fact, it has been shown within the impurity model that interactions with the host system do not contribute greatly beyond the nearest neighbors.[64] This means that, for *ab initio* cluster calculations as well, the small size of the ligand basis is not limiting the quality of the results obtained for the description of the transition-metal ion. The cluster MO+RCT-CI+CEC model and the impurity model applied to clusters have many fundamental simi-

larities. Both point to inadequacies in simpler ligand–crystal-field parametrization schemes. They differ greatly, however, in quantitative execution and in type of information obtained.

V. SUMMARY OF RESULTS

In contrast to earlier semiempirical fittings or estimations of the spectrum based upon the ligand–crystal-field model, *ab initio* SCF MO's have been calculated as a basis for including correlation effects within the *d*-shell electrons and between them and ligand–valence-shell electrons. Particular attention was paid to the sextet ground and quartet excited states seen below the band edge of host II-VI crystals. The methodology used was developed in detail to facilitate recognition of the physical effects treated at the several levels of computation. A number of significant conclusions have been noted.

1. SCF MO's were obtained at three R(Mn-S) distances, including the value in β-MnS, 2.43 Å. From them several features are revealed that depend mainly upon the orbital characteristics of the system.

(a) The fixed (electrostatic) external potential field in which the MnS_4 system is embedded has little effect upon the MO's or excitation energies, although it was included in all subsequent calculations.

(b) The *d*-shell electron density may be characterized as about 3.5% delocalized in the ground state and about 5.5% on average in the excited quartets, at 2.43 Å. Delocalization decreases as R increases. It is slightly smaller with π-type d MO's than with σ types.

(c) Despite the modest change in delocalization, the internal electronic relaxation energy (IERE) for excitation to the quartet states is small (about 0.1 eV). Subsequent calculations included this effect by using the average-energy Hamiltonian $\overline{H}$; it produced the best agreements with experiment.

(d) Ionization and electron attachments to the MnS_4^{6-} cluster (and also intercluster electron transfers), however, produce larger IERE's (4–6 eV) and also large external bulk polarizations of the host, the order of 4 eV. Estimated IP's associated with Mn *d* states agree well with XPS and UPS data for II-VI systems.

(e) The R variation of the ground-state total energy shows a minimum well beyond that observed and the force constant for the a_1 mode is likewise unreliable. Repulsive contributions from ions nearest the cluster are clearly necessary. Their absence, however, does not appear to influence vertical excitation energies.

2. The significance of electron correlation upon the spectrum is clearly revealed even at the LF-CI+CEC level, which encompasses intra-*d*-shell correlation-energy corrections (CEC) formally equivalent to the intermediate CF scheme.

(a) Need for the intra-*d*-shell CEC is seen already at the free-ion level, since the pure orbital [Hartree-Fock (HF)] model cannot reproduce intervals within the observed Mn^{2+} levels. In empirical CF models, these effects are incorporated only by use of the weak-field basis in the intermediate-field scheme.

(b) Since these calculations are based upon MO's, equivalent to the strong-field CF scheme, LF-CI and CEC are essential to obtain even semiquantitative agreements with the observed spectrum. Strong mixing of e^1t^4, e^2t^3, and e^3t^2 configurations is found for the ^4T states; approximate transformations to the free-ion coupling basis shows, however, that all states retain free-ion character except the two lowest $^4T_1$ states, which show considerable ^4G-^4P mixing.

(c) The variation of excitation energies with R is qualitatively similar to the empirical CF diagram, in the region about $Dq = 350$ cm^{-1} and to the width and band positions in the observed spectrum. There are two major differences: (i) the order of $b\,^4T_1$ and $b\,^4T_2$, (ii) the threshold for *d-d* absorption is about 0.5 eV too high.

(d) Near-degeneracy and distance-dependence of transitions to $^4A_1$ and $a\,^4E$ are found, although their order is the reverse of semiempirical predictions.

3. Correlation effects from relaxed-charge-transfer–type excitations from sulfur valence orbitals into the *d* shell have a further and profound influence upon the calculated spectrum. Despite being restricted in extent by size limitations and to $R = 2.43$ Å, these results indicate several important features of the metal-ligand interaction that are not included in the current ligand-field–based models.

(a) Since the CT levels lie above the observed *d* states and furthest from the ground state, they depress the quartets relatively more than $^6A_1$. The overall width of the quartets is unchanged, but the discrepancy in *d-d* absorption threshold is halved.

(b) Significant differential effects within the quartet states also are found. These effects appear to be determined not merely by their relative proximity to the CT levels but more by the amount of the (highest-energy) e^3t^2 configurational component of the interacting *d* state.

(c) These differential effects (nearly) restore the degeneracy of $^4A_1$ and $a\,^4E$ found in the simplest theories; they also reverse the order of $b\,^4T_1$ and $b\,^4T_2$, found at the LF-CI+CEC level and corresponding to the region near $Dq = 1000$ cm^{-1} in the CF diagram. This order agrees with most prior assignments of the observed bands.

(d) These important correlation contributions to excitation energies are accompanied by some backtransfer of electron density to Mn, about 2% in the ground state and 4–6 % in the observed quartets, making the metal formally almost exactly Mn^{2+}.

(e) Difficulties experienced in fitting CF parameters to the experimental spectrum are now understood. In them, unphysically large and arbitrary orbital reduction factors are forced also to represent the *non*orbital, two-electron correlation effects of comparable sizes.

(f) With RCT-CI and CEC added to the basic cluster MO calculation, one has a quantitative procedure that encompasses the same physical features as the qualitative valence-bond model, both of which appear valid in these ionic host crystals.

(g) Although the best calculated excitation energies (Table XI) are still obtained 0.2–0.3 eV too high, these first-principles results are quite gratifying. It seems that

all results would be better if the CT effects were somewhat larger. A more extensive CT-CI calculation, including the larger number of virtual orbitals as in the NiO_6 and Cu halide clusters and better optimization of the MnS_4 CT states, is clearly indicated. Since the S^{2-} ions are more polarizable than O^{2-} or halide, hole-particle localization may be more important in the MnS_4 system. Some further refinement might result also from including non-Coulombic terms in V(ext) and bulk polarization in the basic cluster calculations. Such extensions, however, are unlikely to modify significantly the conclusions drawn from the present results.

ACKNOWLEDGMENTS

This investigation was supported in part by the Netherlands Foundations for Chemical Research [Stichting Scheikundig Onderzoek in Nederland (SON)] with financial aid from the Netherlands Organization for the Advancement of Pure Research [(ZWO)]. We are indebted to Dr. G. Aissing for computational assistance and to Professor W. C. Nieuwpoort for many helpful discussions. J.W.R. appreciates the hospitality provided to him by the Laboratory of Chemical Physics at the University of Groningen while many of the calculations were being performed.

*Present address: Netherlands Energy Research Foundation ECN, P.O. Box 1, NL-1755 ZG Petten, The Netherlands.

[1]For a recent review of data, older theoretical models and discussion of an approach based upon Green's-function methods, see A. Zunger, in *Solid State Physics, Advances in Research and Applications,* edited by H. Ehrenreich, F. Seitz, and D. Turnbull (Academic, New York, 1986), Vol. 39, p. 275.

[2]J. W. Richardson and G. J. M. Janssen, in *Diluted Magnetic Semiconductors,* Vol. 89 of *Materials Research Society Symposium Proceedings,* edited by R. L. Aggarwal, J. K. Furdyna, and S. von Molnar (MRS, Pittsburgh, 1987), p. 203.

[3]Y. R. Lee, A. K. Ramdas, and R. L. Aggarwal, Phys. Rev. B **33**, 7383 (1986).

[4]See the survey by D. R. Yoder-Short, U. Debska, and J. K. Furdyna, J. Appl. Phys. **58**, 4056 (1985).

[5]A. Balzarotti, M. Czyzyk, A. Kisiel, N. Motta, M. Podgorny, and M. Zimnal-Starnawska, Phys. Rev. B **30**, 2295 (1984).

[6]N. Motta, A. Balzarotti, P. Letardi, A. Kisiel, M. T. Czyzyk, M. Zimnal-Starnawska, and M. Podgorny, Solid State Commun. **53**, 509 (1985).

[7]B. A. Bunker, W.-F. Pong, U. Debska, D. R. Yoder-Short, and J. K. Furdyna, Ref. 2, p. 231.

[8]See, for example, L. E. Orgal, J. Chem. Phys. **23**, 1822 (1955).

[9]H. E. Gumlich, P. L. Pfrogner, J. C. Schaffer, and F. E. Williams, J. Chem. Phys. **44**, 3929 (1966).

[10]D. Curie, C. Barthou, and B. Canny, J. Chem. Phys. **61**, 3043 (1974).

[11]S. Koide and M. H. L. Pryce, Philos. Mag. **3**, 607 (1958).

[12]A. Fazzio, M. J. Caldas, and A. Zunger, Phys. Rev. B **30**, 3430 (1984).

[13]R. Parrot and C. Blanchard, Phys. Rev. B **6**, 3992 (1972).

[14]S. Ves, K. Strössner, W. Gebhardt, and M. Cardona, Solid State Commun. **57**, 335 (1986).

[15]L. L. Lohr, Jr., J. Chem. Phys. **55**, 27 (1971).

[16]M. Floréz, L. Seijo, and L. Pueyo, Phys Rev. B **34**, 1200 (1986).

[17]R. Parrot, C. Naud, F. Gendron, C. Porte, and D. Boulanger, J. Chem. Phys. **87**, 1463 (1987).

[18]D. Boulanger and R. Parrot, J. Chem. Phys. **87**, 1469 (1987).

[19]G. J. M. Janssen, Doctoral thesis, University of Groningen, 1986.

[20]T. F. Soules, J. W. Richardson, and D. M. Vaught, Phys. Rev. B **3**, 2186 (1971).

[21]A. J. H. Wachters and W. C. Nieuwpoort, Phys. Rev. B **5**, 4291 (1972).

[22]L. Pueyo and J. W. Richardson, J. Chem. Phys. **67**, 3577 (1977).

[23]K. H. Johnson and F. C. Smith, Phys. Rev. B **5**, 831 (1972).

[24]J. P. Perdew and A. Zunger, Phys. Rev. B **23**, 5048 (1981).

[25]M. R. Norman and D. D. Koelling, Phys. Rev. B **30**, 5530 (1984).

[26]T. Ziegler, A. Rank, and E. J. Baerends, Theor. Chim. Acta **43**, 261 (1977).

[27]J. Hubbard, D. E. Rimmer, and F. R. A. Hopgood, Proc. Phys. Soc. London **88**, 13 (1966).

[28]S. Yu. Shaskin and W. A. Goddard III, Phys. Rev. B **33**, 1353 (1986).

[29]G. J. M. Janssen and W. C. Nieuwpoort, Phys. Rev. B **38**, 3449 (1988).

[30]G. J. M. Janssen and W. C. Nieuwpoort, Int. J. Quantum Chem. Symp. (to be published).

[31]J. S. Griffith, *The Theory of Transition-Metal Ions* (Cambridge University Press, Cambridge, England, 1961).

[32]A. J. H. Wachters, J. Chem. Phys. **52**, 1033 (1970).

[33]P. J. Hay, J. Chem. Phys. **66**, 4377 (1977).

[34]B. Roos and P. Siegbahn, Theor. Chim. Acta **17**, 209 (1970).

[35]G. A. van der Velde, Doctoral thesis, University of Groningen, 1974.

[36]To evaluate directly this tenth integral, called i in Refs. 31 and 37, would have required inconvenient manipulations of the SYMOL program. It is quite small and is approximated to sufficient accuracy by the formula $i \equiv \langle \theta\xi | \eta\zeta \rangle \simeq i_0[K(\theta\eta)K(\xi\zeta)/K_0(\theta\eta)K_0(\xi\zeta)]^{1/2}$, where $\theta;\xi,\eta,\zeta$ are subspecies of the degenerate $e;t$ MO's, respectively, and the subscript 0 indicates values computed from pure $3d$ AO's.

[37]J. W. Richardson, T. F. Soules, D. M. Vaught, and R. R. Powell, Phys. Rev. B **4**, 1721 (1971).

[38]Alternative expressions for the elements are given by R. R. Sharma, M. H. de A. Viccaro, and S. Sunderman, Phys. Rev. B **23**, 738 (1981).

[39]H. Watanabe, *Operator Method in Ligand Field Theory* (Prentice-Hall, Englewood Cliffs, 1966), Appendix 4.3. There are some differences in phasing, compared to Griffith (Ref. 31).

[40]For a recent review of CI methods see H.-J. Werner, in *Ab Initio Methods in Quantum Chemistry, Part II,* Vol. LXIX of *Advances in Chemical Physics,* edited by K. P. Lawley (Wiley, New York, 1987), Chap. 1.

[41]D. Hegarty, in *Proceedings of the 5th Seminar on Computational Methods in Quantum Chemistry, 1981,* edited by P. Th. van Duijen and W. C. Nieuwpoort (Max-Planck-Institut für

Physik und Astrophysik, Garching bei München, 1982).
[42]The result of these considerations is that the T_d point-group–symmetry $^6A_1$ ground state is represented by a linear combination of 3270 CSF's (from ^6A of D_2); the T_d $^4T_1$ and $^4T_2$ states by 22 745 CSF's (from $^4B_1$ of D_2); and the $^4A_1$, ^4E, and $^4A_2$ states by 15 047 CSF's (from ^4A of D_2).
[43]T. Koopmans, Physica **1**, 104 (1933). The formulation applies generally only to closed-shell systems; see footnotes to Table VI for specific formulas valid here.
[44]R. Broer and W. C. Nieuwpoort, Theor. Chim. Acta **73**, 405 (1988).
[45]B. T. Thole and P. Th. van Duijnen, Theor. Chim. Acta **55**, 29 (1980).
[46]C. S. Arguello, D. L. Rousseau, and S. P. S. Porto, Phys. Rev. **181**, 1351 (1969).
[47]C. Webb, M. Kaminska, M. Lichtensteiger, and J. Lagowski, Solid State Commun. **40**, 609 (1981).
[48]N. J. Shevchik, T. Tejeda, M. Cardona, and D. W. Langer, Phys. Status Solidi B **59**, 87 (1973); **60**, 345 (1973).
[49]D. W. Langer, J. C. Helmer, and N. Y. Weichert, J. Lumin. **1**, 341 (1970).
[50]A. Orlowski, K. Kapalko, and W. Chab, Solid State Commun. **50**, 749 (1984).
[51]D. S. McClure, J. Chem. Phys. **39**, 2850 (1963).
[52]V. Luaña, E. Francisco, M. Flórez, J. M. Recio, and L. Pueyo, J. Chim. Phys. **84**, 863 (1987).
[53]V. Luaña, G. Fernandez Rodrigo, M. Flórez, E. Francisco, J. M. Recio, J. F. van der Maelen, L. Pueyo, and M. Bermejo, Cryst. Lattice Defects Amorph. Mater. **15**, 19 (1987).
[54]H. M. Gladney and A. Viellard, Phys. Rev. **180**, 385 (1969).
[55]A. J. H. Wachters and W. C. Nieuwpoort, Int. J. Quantum Chem. **5**, 391 (1971).
[56]J. W. Richardson, D. M. Vaught, T. F. Soules, and R. R. Powell, J. Chem. Phys. **50**, 3633 (1969).
[57]B. Blanchard and R. Parrot, Solid State Commun. **10**, 413 (1972).
[58]J. Zaanen, Doctoral thesis, University of Groningen, 1986.
[59]J. Zaanen, C. Westra, and G. A. Sawatzky, Phys. Rev. B **33**, 8060 (1986).
[60]P. W. Anderson, Phys. Rev. **124**, 41 (1986).
[61]J. Zaanen, G. A. Sawatzky, and J. W. Allen, Phys. Rev. Lett. **55**, 418 (1985).
[62]J. Zaanen, Ref. 58.
[63]G. J. M. Janssen and W. C. Nieuwpoort, Philos. Mag. B **51**, 127 (1985).
[64]J. Zaanen, Ref. 58.